Chapter 1
Physics of Thin Films

Thin film is a material of fine layers formed by the random nucleation and growth processes of individually condensing or reacting atomic, ionic, molecular species on a substrate. The structural, chemical and physical properties of thin films strongly depend on a different number of deposition parameters and its thickness. Thin films may cover a significant thickness range, varying from a few nanometers to tens of micrometers. So it's better to define thin film in terms of the birth processes rather than by thickness [1].

1.1 Introduction

The random nucleation and growth processes bestow new and interesting properties to thin film materials. These properties can be controlled if deposition parameters are optimized up to the requirements. In past era, when fundamentals could not be understood, thin films were named as a 'fifth state of matter' — a state to indicate highly variable properties [1]. The properties of thin films are determined by the type of chemical species they comprise and by film thickness. Their electrical, optical and mechanical behavior is also determined by chemical composition, microstructure, surface and interface morphology, purity and homogeneity. These are strongly dependent on the film fabrication method, chosen parameters, and post-deposition treatments. The materials in the form of thin film show different properties comparatively in bulk form such as optical, electrical, magnetic, thermal and mechanical. Main cause of difference in characteristics of thin film with respect to bulk form is larger surface to volume ratio. The surface and interface properties of substrate can effects thin film properties because of surface mobility, nucleation phenomenon, adsorbed gases, surface topography, contamination, chemical reaction on surface, thermal mismatches and crystallographic orientation [2].

Thin films are produced by different methods such as physical vapor deposition and chemical vapor deposition techniques. A number of various methods are used for fabrication depend upon parameters, which we need for our application. Thin films are commonly fabricated in vacuum by thermally evaporation method or sputtering

technique. In thermally evaporation method, material is heated up to such a high temperature that material evaporates and condenses on a substrate. High vacuum is essentially required to avoid contamination and to get compact films as well. . In sputtering technique, gas ions (usually argon) are bombarded on that target which we want to get in thin film form after sputtering. The main advantage of this technique is that we don't need to heat up the material.

Thin solid films are essential require of this modern technology era. Progress in thin film synthesis regime has given novel electronic, optical, magnetic, ceramic, polymeric and biological materials with improved properties to industrial application need. As for advanced and industrial requirements we need smaller but more efficient, reliable and less expensive devices, which became possible by thin film science technology.

Thin film technology has made expensive progress because of the industrial claim for reliable thin film microelectronic devices. Thin films have plentiful scientific, technical and industrial applications. Metal, insulating, semiconductor and ferromagnetic thin films are used broadly in the electronic industry. Thin films of diverse materials are presently in use as protective and optical coatings [3]. Additional applications, which are most vital for the field of optics and electronics, include polarizers, antireflection films, beam splitters, reflection and transmission type interference filters with narrow and wide bandwidths, radiation detectors and solar energy converters [4]. These examples highlight the diversity of applications for thin films in our modern technology. These also confirm the multidisciplinary research areas on thin solid films.

Modern science and technology is meeting up to the requirements of our need in different regimes. Energy is the basis for economic development. Now people are facing threats to fulfill the energy needs beyond the energy reservoirs. Countries are investing on research and development in the field of renewable energy sources, also keeping in view harmful effect on environment. Within this casing, solar energy technology has taken a particular weight. Thin film processing technologies have direct effect on cost as they are inexpensive, fast and use very small amount of material. For these reasons various materials have been used in the laboratories for making thin film solar cells.

There are several techniques being used to characterize thin films. To characterize we use X-ray diffraction, scanning electron microscopy, spectrophotometer, energy dispersive spectroscopy and atomic absorption etc. These techniques are used to determine the surface morphology, structure, suitability for required application and their composition.

This dissertation particularly represents the fabrication and characterization of CdS and Ag-doped CdS thin films fabricated by close spaced sublimation (CSS) method. The cadmium Sulfide is one of the key materials for thin film solar cells. CdS, belongs to II–VI compound family, has a great application potential such as solar cells, optical detectors and optoelectronic devices. It is a very desirable window layer for many photovoltaic solar cells because of its optical and electrical properties [5]. The results evaluating composition, structure, reflectance, transmittance, band gap, and electrical resistivity are represented in last chapter. An overall review is made at the end.

1.2 Thin Film Formation Mechanism

Growth of thin films from the gas phase is a non-equilibrium phenomenon governed by a competition between thermodynamics and kinetics. Understanding thermodynamics, kinetics and how they relate to each other would enable us to understand that how we can control thin film growth, which is of great importance to basic science and all modern semiconductor technology as well.

1.2.1 Thin Film Growth

Epitaxial growth is an important type of thin film growth, in which the grown film has some crystallographic correlation with the substrate. The main atomic phenomenon, which occur in growth, are shown in Figure 1.1. Vapor atoms reside on substrate, migrate and react with atoms already present and with substrate atoms as well. These interactions define that how morphology of growing film will be.

Evaporated atoms strike the target surface at different positions with different energies. Depending upon their energies, either they adsorb on surface or re-evaporate from the surface. Adsorption of atoms depends upon the type of interaction with surface. Adsorption of atoms may be either by forming a Van der Waal's bond with surface atom

"physisorption" or by forming an ionic or covalent bond "chemisorption". The rate of adsorption of the atoms is roughly proportional to

$$\nu_a exp(-E_a/KT)p_a \text{ ....} (1.1)$$

Where ν_a is the adsorption frequency, E_a is adsorption energy, T is substrate temperature and P_a is the adsorption probability. Because reconstruction of most of the substrates surface are complicated and also binding is directional therefore adsorption probability to some sites is higher than others.

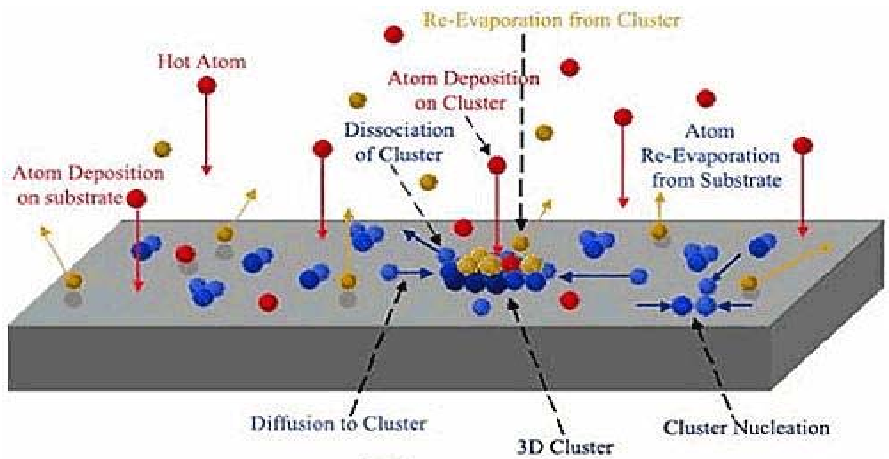

Fig 1.1 Basic phenomenon in thin film growth.

Once atoms adsorbed on the surface can diffuse from one site to other site on surface, by getting thermally activation energy, with diffusion coefficient 'D' [6] such as

$$D \;\alpha\; a^2K_s \;\alpha\; a^2 \; exp(-E_d/kT) \text{ ....} (1.2)$$

Where K_s is the site to site hoping rate, 'a' is the effective hoping distance between sites, E_d is the diffusion energy and 'T' is the substrate temperature. As most of the surfaces have complicated topography in nature so the diffusion is an anisotropic process [7]. Diffusion mechanism also important for the degree of smoothness, of grown film, for a fixed deposition rate. After diffusion ad atoms make bonds with other atoms and get in the form of clusters. Clusters are different in size depend upon the deposition rate or vapor pressure. These clusters then grow to make a continuous film by diffusion control process. However it is important to mention that smooth (ideal) surfaces are not energetically favored for the large number of ad atoms to adsorb and make nuclei. In fact, ideally smooth surfaces don't exist in nature. Defects on surfaces such that, kinks, ledges

and vacancies (Figure 1.2) are favored nucleation sites [8]. Clusters smaller than its critical size (different in different conditions) are energetically unstable, to continue for a stable nuclei, because of large surface-to-volume ratio. Probability of such clusters to dissociate is quite high. Balance between the dissociation and growth of a given cluster depends upon its vapor pressure and total free energy.

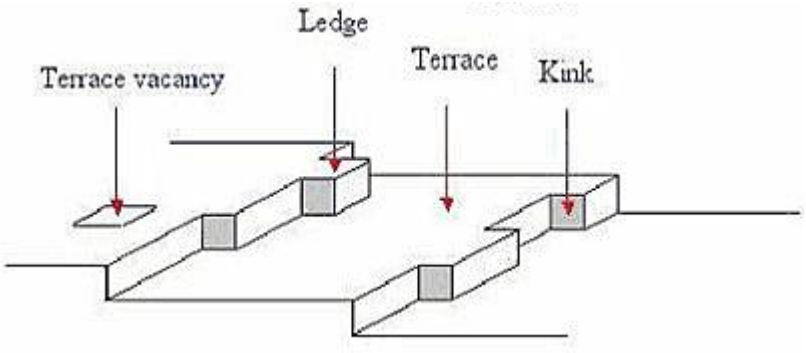

Fig 1.2 Surface defects.

Depending upon the interaction between the atoms of film (suppose to fabricate) and of the substrate, film grows in one out of three forms. If we describe more precisely, it's better to say that modes of film growth depends upon the relation between film surface energy E_A, the substrate surface energy E_B and the interface energy E^* [8]. Figure 1.3 illustrates three different growth modes of film as below:

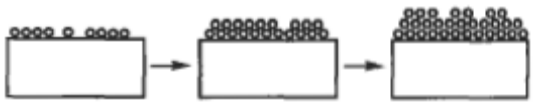

(a) Frank – Van der Merwe (layer-by-layer)

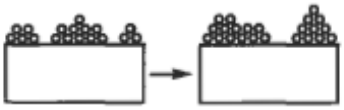

(b) Volmer-Weber (3D island)

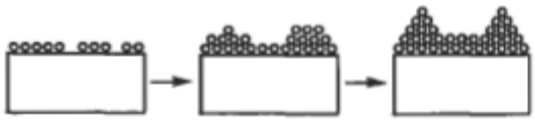

(c) Stranski-Krastanov (layer-plus-island)

Fig. 1.3 Basic modes of thin-film growth.

(1) Frank-Van der Merwe (layer-by-layer): This kind of growth occurs when deposited species have interaction more strongly among themselves than that of interaction with substrate atoms. (i.e. $E_A < E_B + E^*$).

(2) Volmer-Weber (3D island): Takes place when deposited species are less strongly attracted with substrate atoms than among selves. (i.e. $E_A > E_B + E^*$).

(3) Stranski-Krastanov (layer-plus-island): It is an intermediate combination of the aforesaid modes. In this case, after forming one or more monolayers, following layer growth becomes unfavorable and islands form**.**

1.2.2 Summary of Thin Film Formation Mechanism

By observing films formation, with evaporation method, directly in the viewing field of electron microscope it is stated that film growth may be divided into certain stages [9]. Pashley et al. [10] has distinguished four stages of growth process, such as:

(a) Nucleation and island structure.

(b) Coalescence of islands.

(c) Channel filling.

(d) Formation of continuous film.

(a) Nucleation and Island Structure

Nucleation can be called as birth stage of a film. The evaporated species, which we want to deposit, generally lose a part of their energy on impingement to substrate (target). So mobility of the species decreases on surface because of loosing energy. One of the reasons to elevate substrate temperature is, to provide sufficient energy to the atoms to mobilize them which is necessary for the accommodation on the substrate and among themselves [10]. The diffusion of ad-atoms depends upon the interaction between the atoms of substrate and the ad-atoms (adsorbed atoms) and the substrate temperature as well. Defects and crystallographic variations at substrate surface acts as potential well and to keep moving around, atoms have to overcome this potential barrier. In diffusing randomly they join other atoms to form doublets, which have lower diffusivities. Beyond a critical nucleus size (on the order of 10-100 Å), the large nuclei grow at the expense of

smaller ones, so the number of nuclei on the substrate frequently decreases throughout growth. The primary nucleation is enhanced with the presence of defects on the substrate. At this stage individual crystallites (about 100 Å in diameter) are quite perfect structurally. As more flux reaches at the surface, the nuclei sizes grow and eventually islands are formed which often have the shape of small crystals (crystallites).

(b) Coalescence

At this stage some islands come in to contact and coalescence ensues as shown in Figure. 1.4. Coalescence phase is critical for the formation of dislocations and grain boundaries. As larger nuclei coalesce, the degree of disorder at the merging boundary depends on the orientation of each nucleus before they came in contact with each other. If the nuclei are aligned well, either a twin boundary or none at all may be formed. In other case (as in case of an amorphous substrate or growth at low temperature), a grain boundary is created. As the nuclei become larger, the energy becomes smaller so the larger nuclei have less ability to accommodate to each other as they coalesce [11].

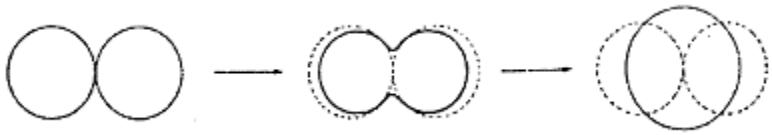

Fig. 1.4 Schematics of coalescence of two nuclei.

After coalescence temperature drops. It has been stated that when two islands of different crystallographic orientation and size coalescence, the resultant crystallite assumes the orientation of larger one [9].

(c) Channel Filling

As islands grow, their tendency decreases to become entirely rounded after coalescence. However shape changes, but in the immediate territory of junction of the islands. Consequently, the islands elongate and join to shape a continuous structure in which the deposit material is separated by long, irregular, and narrow channels [12]. With further deposition, secondary nucleation occurs which fills these channels after growth. At the same time, channels are bridged at some points and fill in quickly in liquid like

manner. Eventually, most of the channels are eliminated and the film approaches to continuous fashion but contains several small irregular holes

(d) Formation of Continuous Film

Secondary nucleation takes place with in holes, which are produced during channel filling stage. Holes contain many secondary nuclei which coalesce to form secondary islands which approach circumference of hole and coalesce with the main film to leave a clean hole. Further secondary nuclei form, and the procedure is repeated until the hole fills. The liquid like behaviour occurs until a complete film is formed [12]. These processes are shown in Figure. 1.5

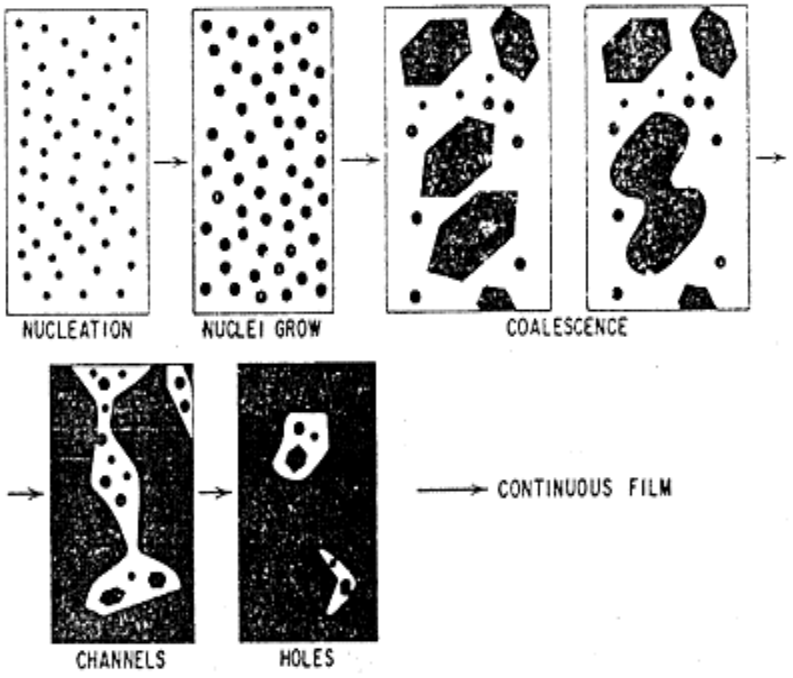

Fig. 1.5 Stages of film growth.

1.3 Adhesion of Thin Films

The adhesion of thin films to a substrate is a significant property in more or less all applications. It depends on the nature and the strength of the binding forces between the film and substrate [9]. Two major type of adhesion mechanism are discussed as below:

1.3.1 Chemical Adhesion

Two different types of materials may form a compound where they join. Chemically two types of join may occur. The stronger one is where atoms of two materials swap (ionic bonding) or share (covalent bonding) outer electrons. A weaker bond is formed if the atoms of nitrogen, oxygen or fluorine of two materials share a hydrogen nucleus (hydrogen bonding).

1.3.2 Dispersive Adhesion

It is stated that the van der Waal's forces also cause adhesion which is recognized as dispersive adhesion or adsorption. A Van der Waal's force is developed when two molecules having positively and negatively charged ends are attracted. The strength of the adhesion between substrate and thin film depends on which of the above mechanisms occur between the two, and the surface area over which they become in contact. A qualitative guess of degree of adhesion is made by the scotch tape test, in which the film to be tested is lifted off the substrate by adhesive tape. Different film abrasion techniques are also used, their results being dependent on the hardness of the film [9].The ratio between the rate of adsorption to the rate, at which the adsorptive species reaches at the total surface, i.e., covered and uncovered, is called the 'sticking coefficient'. It is generally a function of surface coverage, temperature and the surface morphology of the adsorbent. Degree of adhesion is estimated generally by scotch tape test, in which the film is lifted off from substrate by adhesive tape.

1.4 Substrates

In thin film fabrication, substrates serve as mechanical support for deposited film. In different applications substrates also serve in different ways, like in electronic applications substrates semi conductor thin films serve as an insulator. If we desire to enhance life and to maintain properties of thin film for a long time then we have to use such a substrate which would not react with thin film. Therefore substrates must fulfill certain requirements regarding their adhesion and stability, not only at ambient environment but also in different variable conditions (e.g. at higher temperature). These variable conditions may occur during fabrication of thin films as well as where these are to be used further. To maintain surface evenly heated, appropriate thermal conductivity is

required. To fabricate thin films of our required parameters, surface of the substrate should be smooth and flat.

In general, it is rite to say that no substrate fulfills all requirements up to standards. For single crystal epitaxial growth, most frequently materials used for substrates are the single crystals of silicon, alkali halides, mica and sapphire. In polycrystalline thin films, most widely used substrates are glass, fused silica, ceramics and polymers as well in some cases. Pyrex or fused silica, which can with stand at variable degrees of temperature, is also chemically inactive. Alkali contents of different types of glasses are very important regarding their properties. Substrates with higher alkali contents are often the cause of instability in the electrical and other physical properties. Surface of glass substrates are relatively more flat and smooth rather than ceramics or other substrates. Ceramic substrates are less smooth and flat but these have advantage of having higher mechanical strength, better thermal resistance and conductivity. The surfaces of single crystals may be made smooth at atomic scale by cleavage, for example in case of mica. Some time substrates having rough surface (up to some limits) are considered better for adhesion of deposited material. As described earlier that no substrate of any materials can be perfect ideally up to our requirements, so we have to compromise one some parameters. The surface of alkali halides shows step (atomically small), which serve as nucleation centers on which the most part of deposited material condense. Regarding smoothness and transparency point of view glass is a better choice of substrate. In our case of thin film deposition, we used corning glass as a substrate.

1.4.1 Atomic Picture of Substrate and Film Growth

An idealized atomic picture of a substrate surface during thin film growth is shown in Figure 1.6. When atoms reach at substrate surface they have two degree of freedom. Atoms at the steps (one degree of freedom) or at kinks have, on the average, less energy than those on the flat surface. Mobility of the atoms on the surface decreases because they loose their energy to the substrate while striking the surface. The need of elevated substrate temperature is to provide sufficient energy to atoms so that they can

make necessary movements for the accommodation at the substrate and among themselves [11].

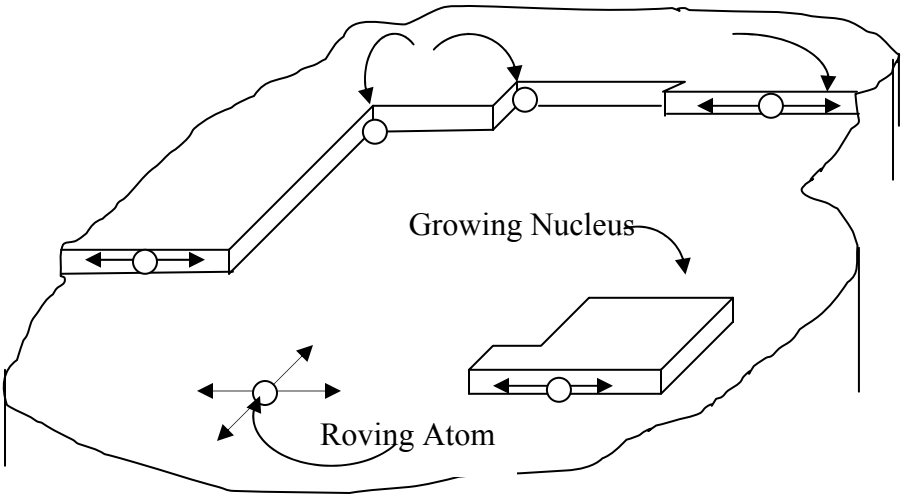

Fig. 1.6 Idealized schematic of substrate during initial stages of deposition.

Normally the portion of the film nearby the substrate is relatively most disordered, since this is where impurity defects and lattice matches are accommodated as shown in Figure 1.7.

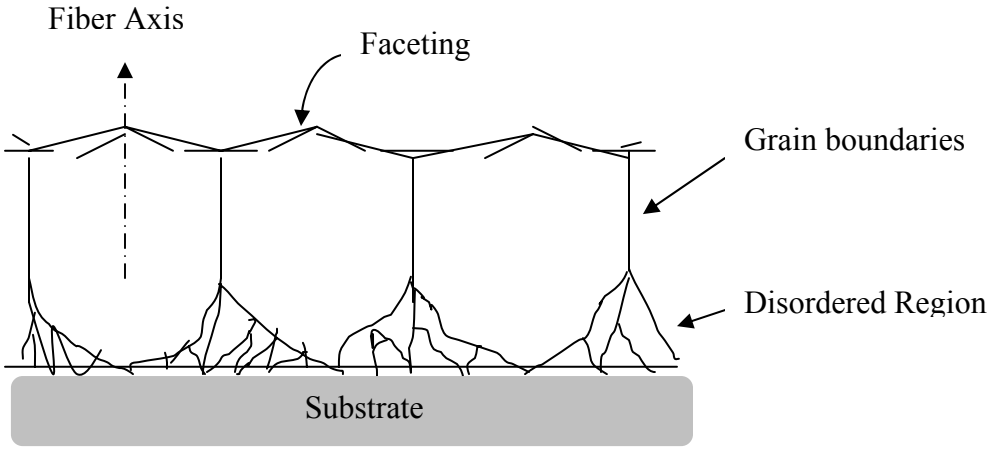

Fig.1.7 Schematic cross section of poly crystalline thin film grown on amorphous substrate [11].

As long as film grows and becomes thicker, difference in growth rate of different crystal faces produce faceting on each of the grains. Since large crystallites grow at the expense

of smaller ones by crowding them out as columnar grain, producing a fibrous texture in the film. Finally, the surface of the film has a texture of dimension of the order of the grain size due to faceting during growth [11].

1.5 Semiconductor Materials

A semiconductor is a solid state substance whose electrical properties can be altered. By definition, a solid material whose electrical conductivity at room temperature is between that of a conductor and that of insulator is known as semiconductor. Its electrical conductivity approaches to metal at high temperature and approaches to insulator at low temperature. In terms of energy bands, semiconductors can be defined as those materials, which at room temperature have, partially filled conduction and valence band and very narrow energy gap (of the order of 1 eV) between them.

Useful feature of a semiconductor material is that its electronic properties can be altered (up to some extent) regarding our application point of view, with doping of impurities. Search for new semiconductor materials and improvement in their properties is a vast field of research because of their applications in semiconductor industry. These are generally classified as elemental and compound semiconductors. Any semiconductor material consisting of two or more than two, like material from I and III groups or II and VI groups of elemental periodic table will be called compound semiconductor. These columns (I, II, III etc.) indicate groups of elements having similar properties.

1.5.1 II-VI Semiconductors

It has been thought that silicon is to electronics what steel is to mechanical engineering [13]. Steel is successfully used for most of the world's construction but there are some tasks to which it is incapable and for which substitute materials are better suited. In the same way there are some vital applications – such as optoelectronics and very high speed electronics – that silicon are generally suitable but for which a broad range of compound semiconductors are better equipped to perform. Binary and ternary compounds are being used in many applications because of their wide range of optical and electrical properties. These properties make them substitute candidate of silicon and of other materials in optoelectronic and photovoltaic applications. Alloy of II-VI

compounds are potential candidates for opto-electronic device applications [14]. Below is a list of II-VI compound semiconductors:

- Cadmium Sulfide (CdS)
- Cadmium Selenide (CdSe)
- Cadmium Telluride (CdTe)
- Zinc Sulfide (ZnS)
- Zinc Selenide (ZnSe)
- Zinc Telluride (ZnTe)
- Zinc Oxide (ZnO)

1.5.2 Cadmium Sulfide Thin Films

CdS belongs to II–VI compound family, has a great application potential such as solar cells, optoelectronic devices and optical detectors [15-17]. It is very appropriate window layer for many photovoltaic solar cell modules because of its electrical and optical properties [18-21]. Research on CdS has been an intensive subject because of its band gap, reasonable conversion efficiency, high absorption coefficient, stability and low cost [22]. Investigation about current transport mechanisms in CdS thin films has been reported in detail [23] and there exists a vast literature encompass theoretical and experimental study of electronic band structure [24]. CdS is wide and direct band gap (2.42 eV) n-type semiconducting material [25]. CdS exists in two crystalline forms: phase cubic (zincblende) phase and hexagonal (wurtzite) phase, and it is possible to grow CdS films in both these phases. The development of cubic or hexagonal phase depends on many features including the deposition technique [26]. CdS thin films are being used commonly as window material in high efficiency CdTe and other polycrystalline thin film photovoltaic devices [27]. Efficiencies about 16% have been stated for CdTe/CdS thin film solar cells [28]. Generally undoped CdS thin films have high electrical resistivity. To reduce resistivity of CdS films, different dopants are being used. CdS thin films can be deposited by different deposition techniques such as thermal evaporation, chemical bath deposition, vacuum evaporation, chemical vapour deposition, spray pyrolysis, metal

organic vapour-phase epitaxy, close space sublimation, photochemical deposition, radio frequency sputtering, vapour transport deposition, electro deposition, screen printing and pulsed laser deposition, etc[29-37].

1.6 Thin Film and Semiconductor Devices

Thin film technology serves an important role in industrial applications. This technology was developed mainly for the requirement of 'integrated circuit' industry. To develop devices with smaller size and higher speed particularly in new generation of integrated circuits requires sophisticated materials and advanced processing techniques appropriate for giga scale integration (GSI) technology in future. In this regard, the production of thin films for device engineering has been developed over the past 40 years. Thin films have great importance to solution of many real-world problems as a two dimensional system. They cost very small as compared to the corresponding bulk systems and they execute the similar function when it comes to surface processes. When we decrease thickness of thin films up to some particular orders, generally these show new exotic physical properties. Thus functions and novel properties of thin films can be utilized for the development of new technologies and applications.

Thin film technology is based on three foundations: Fabrication, characterization and applications. Regarding different applications, thin films generally can be categorized as below [2].

1.6.1 Electronic Devices

The fabrication of electronic components, particularly solid-state devices and microelectronic integrated circuits, has definitely found great importance in regime of thin film depositions. These films typically consist of semiconductor materials, metals and insulators.

1.6.2 Electronic Displays

For interfacing electronic equipment with human operators electronic displays are used, in which different components and device structures are necessary, such as:

- Light-emitting diodes (LEDs)

- Liquid-crystal displays
- Plasma and florescent displays
- Electro chromic displays
- Electroluminescent displays

The fabrication of these displays requires conductive and transparent films, dielectric and insulating layers as well as luminescent or fluorescent films.

1.6.3 Optical Coatings

Optical coatings are needed in many applications, like for antireflection purposes, for laser optics, as interference filters on solar panels and as plate glass infrared solar reflectors. In the fabrication of optical filters, thin films with gradient refractive indexes are deposited on pre-forms from which the optical fibers are drawn. In such coatings, dielectric materials with accurately defined indices of absorption and refraction coefficients are required. To increase the luminous flux intensity of filament lamps, infrared reflecting coatings are applied. Laser optics requires metal reflective coatings, which can withstand high radiation intensities without degradation

1.6.4 Magnetic Films for Data Storage

Thin films of magnetic materials have broad commercial applications for data storage in computers, control systems and memory devices. The substrates can be glass, metal or of polymeric materials.

1.6.5 Optical Data Storage Devices

Thin films have rising commercial use for optical data storage devices in computer memory applications and compact disks. Techniques for the deposition of organic polymer materials as storage media and as protective layers are required for this technology.

1.6.6 Antistatic Coatings

To provide protection from electrostatic discharges, thin films of conductive or semi-conductive materials are deposited.

1.6.7 Hard Surface Coatings

Thin films coatings of carbides, nitrides, borides and silicates are widely used to enhance the wear characteristics of surfaces of metallic tools, bearings and machine parts. Because of different characteristics like heat dissipation, hardness and resistance to high-temperature, electrical insulation, and high-energy radiation, diamond-like carbon films have great impact in many applications.

1.6.8 Energy Generation

Energy crises led scientists and developers to search for renewable energy sources. Solar cells are the emerging source of energy these days. A vast area of research is devoted to enhance their efficiency. Solar cell is basically a semiconductor device which converts incident light (photon) directly into electrical power (volts) working on the "photovoltaic effect" principle. PV devices have been used for miscellaneous applications including power supply for space applications, for small electronic device and for electric power in distant locations which are not linked to the supply grids [38]. Different modules are being used in solar cell technology, in which 2^{nd} generation/thin film solar cells have very encouraging results. Crystalline/polycrystalline silicon solar cells are reported as most efficient solar cells till now [39]. Currently CdTe/CdS thin film solar cells module has very encouraging results [40].

References

1. K. L. Chopra, Prog. Photovolt: Appl. **12** (2004) 69.
2. K. Sheshan, Hand Book of Thin Film Deposition Processes and Techniques, Intel corporation, California (2000).
3. L. L. Kazmerski, Polycrystalline and Amorphous Thin Films and Devices, Academic Press, New York, (1980).
4. Hass, Physics of Thin Film, Academic Press, New York & London, (1963).
5. F. Atay, V. Bilgin, Materials Science in Semiconductor Processing **6** (2003) 197.
6. W. Theis and R. M. Tromp, Phys. Rev. Lett. **76** (1996) 2770.
7. G. Brocks and P. J Kelly, Phys. Rev. Lett. **76** (1996) 2362.
8. J. A. Venables, Introduction to Surface and Thin Film Processes, Cambridge University Press (2000).
9. L. Eckertová, Physics of Thin Films, Plenum Press, New York, (1977).
10. D. W. Pashley, M. J. Stowell, M. H. Jacobs and T. J. Law, Phil. Mag. **10** (1964) 127.
11. A. L. Fahrenbrach, R. H. Bube, Fundamental of Solar Cells, Academic Press, Inc. New York (1983).
12. L. I. Maissel, R. G. Lang, Handbook of Thin Film Technology, McGraw Hill, Inc. (1970).
13. H. Kroemer, Nobel Lectures in Physics, Imperial College Press, London (2000).
14. S. D. Cobb, F. R. Szofran, K. S. Jones and S. L. Lehoczky, J. Electron. Mater. **28** (1999) 732.
15. R. Tenne, V. M. Nabutovsky, E. Lifshitz, A. F. Francis, Solid State Commun. **82** (1992) 651.
16. V. Ruxandra, S. Antohe, J. Appl. Phys. **84** (1998) 727.
17. B. Su, K. L. Choy, Thin Solid Films **102** (2000) 361.

18. A. G. Valyomana, K. P. Vijayakumar, C. Purushothaman, J. Mater. Sci. Lett. **11** (1992) 616.
19. H. Chavez, M. Jordan, J. C. McClure, G. Lush, V. P. Singh, J. Mater. Sci. **8** (1997) 151.
20. F. Izci, S. Kose, K. Yckaya, Proc. Suppl. Bpl. **5** (1997) 1115.
21. A. G. Valyomana, K. P. Vijayakumar, C. Purushothaman, J. Mater. Sci. Lett. **9** (1990) 1025.
22. S. A. Al Kuhaimi, Vacuum **51** (1998) 349.
23. I. Gunal, M. Parlak, J. Mater. Sci. **8** (1997) 9.
24. U. Pal U, R. Silva-Gonzalez, G. Martinez-Montes, M. Gracia Jimenez, M. A. Vidal, S. Torres. Thin Solid Films **305** (1997) 345.
25. H. Zhang, X. Ma, D. Yang, Mater. Lett. **58** (2003) 5.
26. J. Pantoja, X. Mathew, Solar Energy Materials & Solar Cells **76** (2003) 313.
27. M. E. Ozsan, D. R. Johnson, M. Sadeghi, D. Svapathasundaram, G. Goodlet, M. J. Furlong, L. M. Peter, A. A. Shingleton, J. Mater. Sci. **7** (1996) 119.
28. N. Romeo, A. Bosio, R. Dedeschi, V. Canevari, Thin Solid Films **327** (2000) 361.
29. R. N. Ahmad-Bitar, Renewable Energy **19** (2000) 579.
30. H. Ariza-Calderon, R. Lozada-Morales, O. Zelaya-Angel, J.G. Mendoza, L. Banos, J. Vac. Sci. Technol. **14** (1996) 2480.
31. S.J. Ikhmayies, Production and Characterization of CdS/CdTe Thin Film Photovoltaic Solar Cells of Potential Industrial Use, Ph.D. Thesis, University of Jordan, 2002.
32. O. Vigil, I. Riech, M. Garcia-Rocha, O. Zelaya-Angel, J. Vac. Sci. Technol. 15 (1997) 2282.
33. O. Melo De, L. Hernan ´ dez, O. Zelaya-Angel, R. Lozada-Morales, M. Bercerril, E. Vasco, Appl. Phys. Lett. **65** (1994) 1278.
34. M. Lepek, B. Dogil, Thin Solid Films **109** (1983) 103.
35. B. Ullrich, R. Schroeder, IEEE J. Quantum Electron. **37** (2001) 1363.
36. H. Wang, Y. Zhu, P.P. Ong, J. Cryst. Growth **220** (2000) 554.
37. M. Khanlary, P. Townsenda, B. Ullrich, D.E. Hole, J. Appl. Phys. **97** (2005) 23512.

38. L. D. Partain, Solar Cells and Their Applications, New York, Wiley (1995).
39. R. H. Bube, Photovoltaic Materials, Imperial College Press (1998).
40. P. Sagan, G. Wisz, M. Bester, I. O. Rudyj, I. V. Kurilo, I. E. Lopatynskij, I. S. Virt, M. Kuzma and R. Siach, Thin Solid Films (2005) 318.

Chapter 2
Deposition Technique and Experimental Setup

There is a broad range of techniques for the deposition of thin films. Each technique has different characteristics, on which it is decided that which deposition method will be better for thin film of our required properties. Deposition methods fall into two major types [1], as follows:

- Chemical Methods
- Physical Methods

2.1 Chemical Methods

In Chemical methods, generally process is faster and economical, with simpler equipments. However these methods are difficult to control and complex as well [2]. During the process, side reactions occur and it is difficult to fabricate thin film of same properties. In chemical methods, some techniques require conditional substrates such that substrates with exposure to higher temperature or different solvents. Such complications have reduced the applications of this method [2].

There are several deposition techniques which come under the tag of chemical method [3].

- Chemical Vapor Deposition
- Electro-deposition or Electroplating
- Anodization
- Electro-less plating
- Immersion plating
- Electrophoretic Coatings

2.2 Physical Methods

Physical methods are commonly called as physical vapor deposition (PVD) methods. There are two major categories of physical methods.

(1) Sputtering.

(2) Thermal Evaporation.

There are various applications of PVD methods which range from beautification to the high tech appliance. The thickness of the deposited films can vary from 10nanometers up to several microns. By using PVD methods, Very high deposition rates (25um/s) have been achieved. There is a broad range of inorganic materials, compounds, alloys and mixtures as well as some organic materials which can be deposited by using PVD techniques.

2.2.1 Sputtering

In this technique, ejection of surface atoms occurs as a result of train of collision events in the target (which is supposed to deposit) by bombardment of energetic particles. The ejected or sputtered atoms are condensed on a substrate to form a thin film. The number of atoms or molecules ejected from a target surface per incident ion (energetic particle) is called as sputter yield or characteristic of efficiency of sputtering. Sputter yield depends upon many factors.

- No. of atoms displaced toward the surface per primary collision.
- No. of atomic layers that contribute to sputtering.
- No. of target atoms per unit area.
- The cross-section δ_o that depends on Bohr radius of the atom and atomic numbers of the incident and target atoms.

There are some important facts regarding sputtering mechanism, given below:

- There is a “threshold energy” below which sputtering does not occur no matter how high the bombarding flux is.

- Many sputtered atoms have kinetic energies much higher than those of thermally evaporated atoms.
- In a polycrystalline material some crystallographic planes are sputtered faster than that of others (preferential sputter etching).
- Atoms sputtered from an alloy surface are deposited in the ratio of the bulk composition, not their relative vapor pressures as is the case in thermal vaporization.
- There is no sputtering by electrons even at very high temperatures.

In the simplest arrangement for sputtering, the material (target) to be sputtered is used as a cathode in a system containing inert gas (e.g. argon or xenon) at a pressure of 10^{-1}-10^{-3} torr and a voltage is kept up to several kilovolts. The substrate at which the (material) film is to be deposited is placed on the anode of the system. The ions of gas strike with high speed (depends upon applied voltage) and sputter the target, which deposit at the substrate surface atom by atom. There are several techniques [2] available for sputtering; some of them are as under.

- DC Sputtering
- RF Sputtering
- Ion Beam Sputtering
- Glow Discharge Sputtering
- Magnetron Sputtering
- Reactive Sputtering

2.2.2 Thermal Evaporation

In this technique, material which is supposed to be deposited is heated until it vaporizes. The vaporized material condenses on the chamber walls and on the cold substrate surface. The number of particles having molecular weight M, evaporated at temperature T per unit time from clean surface of unit area is given by using kinetic molecular theory[4-6]:

$$N_e = 3.513 \times 10^{22} \; P_e(\text{torr})/\sqrt{MT} \quad molecules\ cm^{-2}\ s^{-1} \ldots\ldots\ldots\ldots\ldots\ldots (2.1)$$

Where P_e is the equilibrium vapor pressure (torr).

To avoid the contamination and side reactions/interactions with unwanted atmospheric species, usually low pressure (up to10^{-6} torr) environment is created in chamber. The portion of species scattered by collision with residual gases is [7-10]. proportional to

$1-exp(-D/\lambda)$

where D is space between source and substrate, λ is mean free path. As at these values of low pressures, mean free path increased as high as evaporated species travel from source to substrate (target) without mutual collisions. The average energy of thermally evaporated atoms, on reaching substrate, is generally low (order of KT). This factor affects the morphology of the films.

To thermally heat the material, there are several different methods are being used such as resistive heating and electron beam heating etc. In thermal evaporation techniques, different methods can be applied to heat the material. Thermal evaporation technique is further divided as follows [1]:

- Resistive Heating
- Flash Evaporation
- Radiation Heating
- Laser Evaporation
- Exploding Wire Technique
- R.F Heating
- Electron Beam Heating
- Two Source Evaporation Technique
- Close Spaced Sublimation (CSS)

Physical vapor deposition (PVD) technique is being used widely to achieve the better properties of prepared materials. Materials formed by sublimation-condensation method reveal well-defined preferential orientation [11]. By using thermally evaporation method, we have deposited CdS (powder form) on glass substrates with close spaced sublimation technique, which is described in detail below:

2.2.3 Close Spaced Sublimation (CSS)

2.2.3.1 Sublimation

Sublimation is a type of evaporation process which can be distinguished in such manner, that species in a solid form gain enough energy to enter directly from solid state to gaseous state without passing through liquid state. Materials which have such a high vapor pressures get into vapor form by absorbing sufficient energy before melting occurs. These vapors then condense on relatively less heated spots (substrate) to form thin film [12].

2.2.3.2 Close Spaced Sublimation (CSS)

The close spaced sublimation technique is a setup with very simple deposition process and it offers high transport efficiency under wide ranges of temperature and pressure (vacuum). The nomenclature 'close spaced' indicates that substrate and source are very close to each other in this assembly. However, the distance between source and substrate is variable (5~20mm) up to our requirements. The source (boat) and (support for) substrate are made up of graphite because graphite is stable at high temperature which is favorable to avoid contamination. Different sources can be used for providing temperature but in our case we used halogen lamps. Source is kept at higher temperature than substrate. The whole assembly of CSS, was setup in Thermal Transport Laboratory SCME, NUST, Islamabad and its block diagram is shown in Figure 2.1.

In CSS process, source materials (boat) can be provided in different forms like single crystal, poly crystalline source block and thin layer. Single crystal is an expensive choice as a source material so thin/thick layer source is favorable because it will lower the cost and can be reproduced with similar composition. Some significant characteristics of our CSS deposition unit are:

1. The system is not complicated and very easy to handle.
2. It provides high transport efficiency under different temperatures and vacuum conditions.
3. One of the significant advantages of CSS assembly is that, there is low loss of evaporated material because of close space between source and substrate.
4. The space between source and substrate can be changed easily up to our requirements (5~20mm).
5. A mica sheet of about 1-2mm thickness is used between source and substrate. It helps out to keep source and substrate at different temperatures, which is necessary for the evaporated material to have better access of substrate. Setup of mica sheet also confines the vapors to a closed space.
6. Heat is provided directly to source and substrate and temperature is controlled with help of temperature controllers.
7. The films deposited by CSS method show a high crystallographic orientation and adequate optical and electrical properties for applications in photovoltaic.
8. Time consumed for the deposition of thin film in it is lesser as compared to two-sourced evaporation method because of lesser time required to evacuate the chamber.

2.2.3.3 Limitations

- The major disadvantage of our deposition unit is that shutter between source and substrate is not installed. Because of which species get start to deposit before our experimental time limit, means we have no control on duration of deposition time.
- In our case (CSS method), evaporation rate is not under control.
- Film thickness can not be controlled precisely.
- To check growth rate we have not any monitoring system.
- In our system, only one film (sample) can be prepared at a time and can only be used only for those materials which can be sublimed.

2.3 Experimental Setup

2.3.1 Coating Unit

In our research work, we also developed our own coating unit at Thermal Transport Laboratory, School Of Chemical and Materials Engineering, NUST, Islamabad. However because of time factor we fabricated thin films on the similar unit at COMSATS. The schematic diagram of apparatus is shown in Figure 2.1. In Figure 2.1 graphite boat is also shown, which we used as a source.

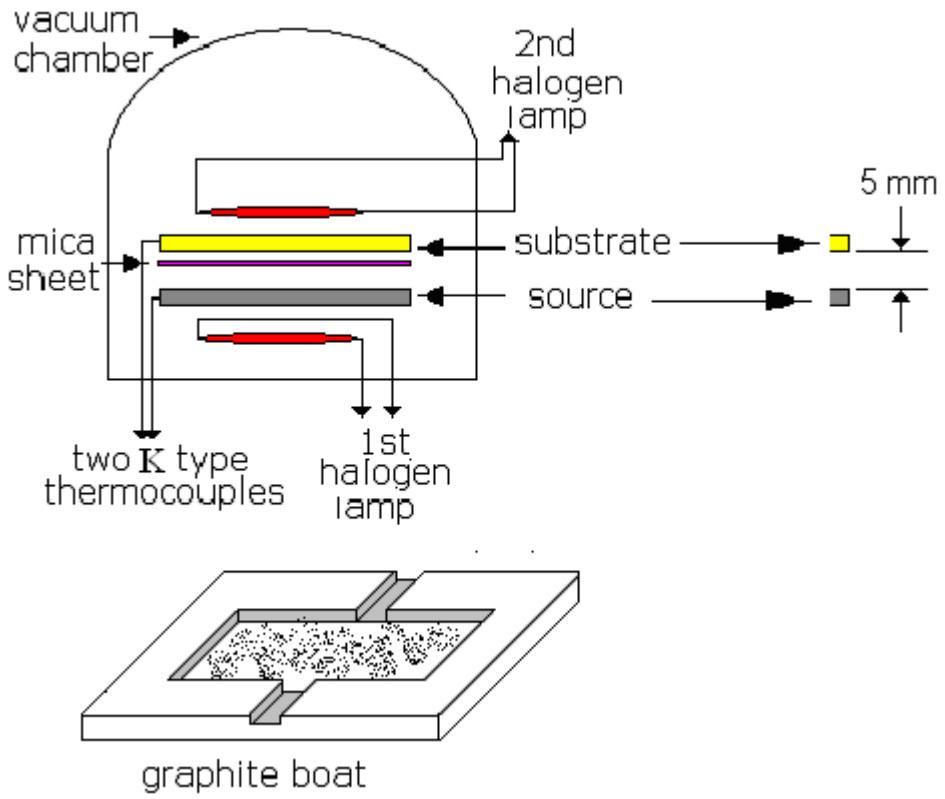

Fig. 2.1 Schematic diagram of thin film fabrication system for CSS method developed at Thermal Transport Laboratory SCME, NUST.

The whole assembly contains different components, given as:

1) Vacuum enclosure

2) Pumping system

3) Source holder with heating arrangement

4) Substrate holder with heating arrangement

An overall view of complete assembly is given in Figure 2.2.

Let us explain different parts of whole CSS unit one by one.

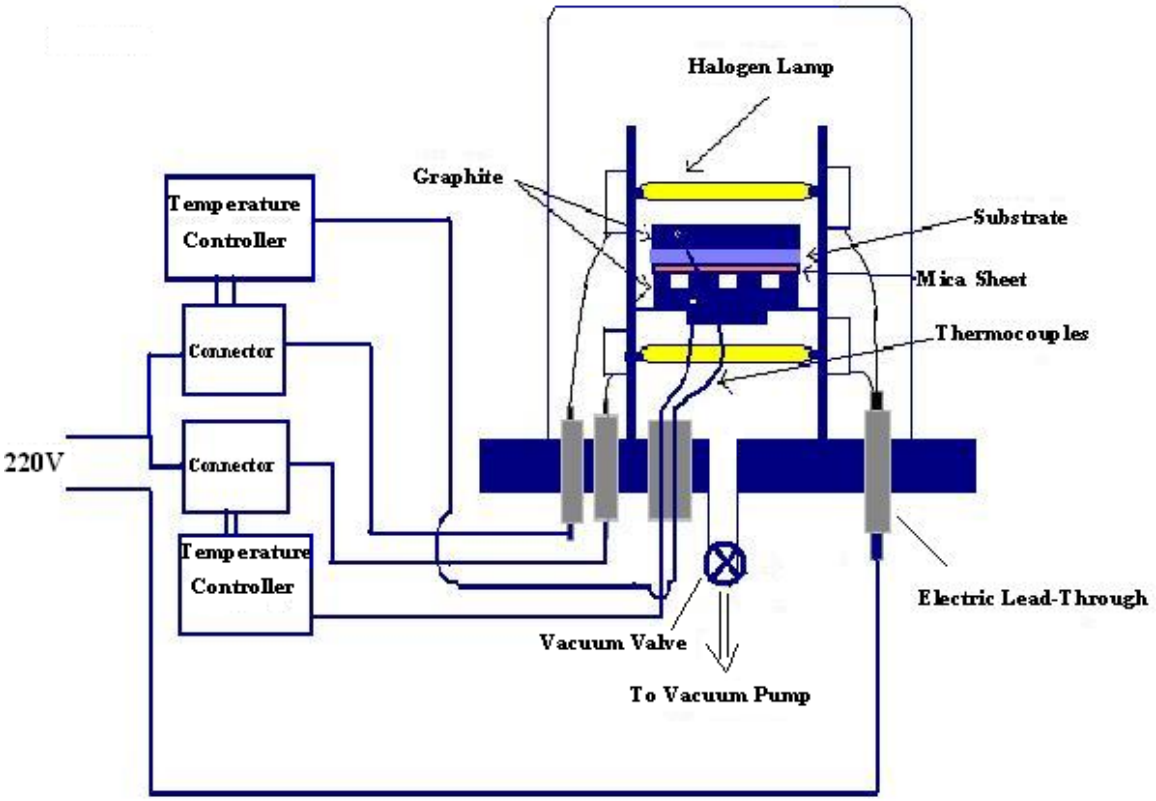

Fig. 2.2 Block diagram of the whole assembly of CSS coating unit.

2.3.2 Vacuum Enclosure

The vacuum enclosure can be of different type, shape and material which could withstand at high temperature and pressure (vacuum) conditions. In our system we used a special type of thick glass of dump (bell jar) shape mounted on a metal base plate, which can withstand at high vacuum 10^{-7} mbar and temperature ~1200^{0}C. The need of vacuum enclosure is to provide contamination free environment without disturbing experimental conditions. To avoid contamination, we need high degree of vacuum so that evaporated species may reach to substrate surface without collisions with gas molecules, i.e. mean free path of the gas molecule increases with reducing the pressure inside the chamber. The approximate pressure inside the chamber should be at least 10^{-2} mbar.

The formula which gives the mean free path of the gas molecules is:

$$L = 5 \times 10^{-3}/P \ldots\ldots\ldots\ldots\ldots\ldots\ldots\ldots\ldots\ldots\ldots\ldots (2.1)$$

i.e. mean free path is inversely proportional to the pressure [1].

The second condition is that we need such a high temperature, so that material which is supposed to be evaporated can evaporate after getting sufficient energy and may reach to substrate surface. So vacuum enclosure has to survive at higher degrees of temperature as well.

2.3.3 Pumping System

Pumping systems depend upon our range of vacuum, required for experimental conditions. We used double-stage rotary vane pump in our case for producing intermediate level vacuum inside the enclosure. Cross-sectional diagram is shown in figure 2.3. It may have single or multiple pumping stages. The range varies (in size) from several hundred cfm (cubic feet per minute displacement) to a fraction of a cfm and are commonly powered by an electric motor operating through a gear or belt drive.

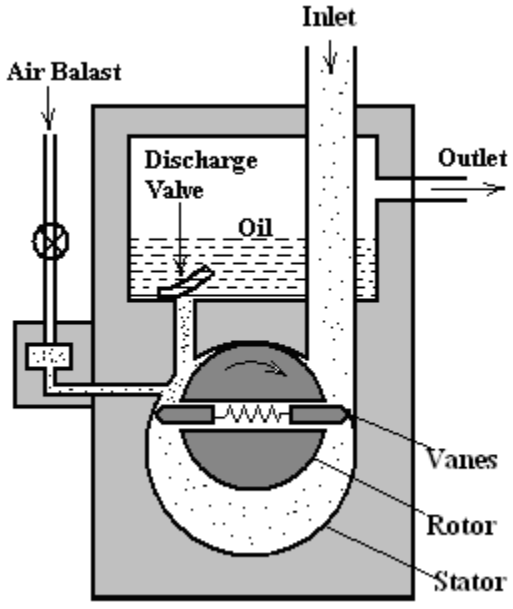

Fig. 2.3 Rotary Vane Mechanical Pump

The working principal is simple and clear-cut. Volume of gas is entrapped in a space enclosed by the stator and the rotor and/or its vanes. As rotor revolves the trapped volume is compressed and transported from the inlet to outlet. As gas is compressed, the pressure increases until an outlet valve opens and the gas exhausts to the atmosphere. The stages are connected internally in double-stage pump. At high intake pressures, the two stages operate in parallel while at lower intake pressures, they operate in series. The practical low-pressure limit for a two-stage mechanical pump is 10^{-3} torr. The rotary pump is oil sealed. The oil serves the dual purpose; it provides a vacuum-tight seal and lubricates the rotating elements. To use only recommended oils for mechanical pump service is important for the life of pump. There are some precautions which are to be considered while working with pumps such as; to check the oil level, to check the direction of rotation before starting first time, to check properly condition of oil of pump and to run the pump at allowed conditions of pressure (vacuum) ranges.

2.3.4 Source Holder and Heating Arrangement

To evaporate the material, we need a source holder (boat). We put our material in source holder to provide it heat so that material may get into form of vapors after absorbing sufficient heat (energy). Now to choose material of source holder is critical because there are chances of contamination from source holder. So we have to choose such a material for source holder which can with stand at very high temperature and pressure (vacuum) conditions. In our system, a source holder specially designed from a graphite block is used, as shown in the figure 2.2. The (boat) source holder, in which the material is kept, is heated by heat radiations from halogen lamp. A hole is drilled on one side of the source holder for inserting thermocouple, which is further connected to an automatic temperature controller. Temperature controller, controls the halogen lamp by switching it ON and OFF on our required values of temperatures. Infect the power of halogen lamp is controlled by temperature controller, which keeps the required temperature of the source holder and of the material inside it. The source holder along with heater arrangement is shown in Fig. 2.4.

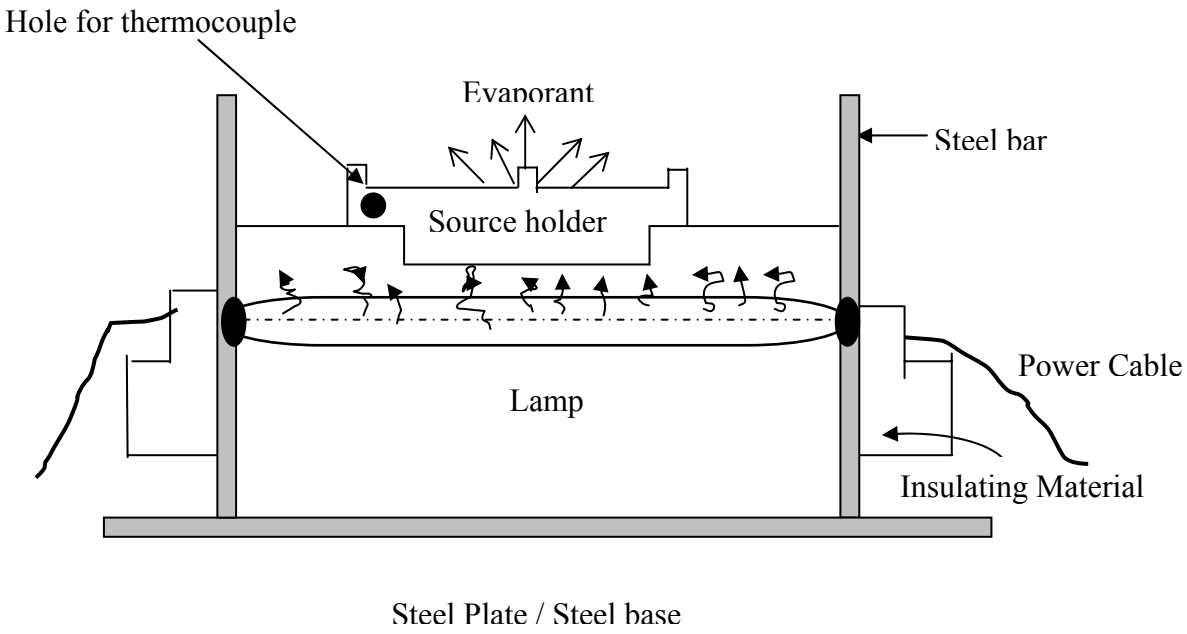

Fig. 2.4 Source holders with heating arrangement

The schematic diagram of graphite boat or source holder is also shown in Fig. 2.1.

2.3.5 Substrate Holder and Heating Arrangement

To fix the substrate well, it is kept on a mica sheet (interconnected 3-4 layers), which serves as dual purpose. It fixes the substrate in the assembly of mica sheet which is prepared according to size of substrate. It is used also as an insulator to avoid the substrate from direct contact with source holder so that temperature difference between source and substrate is made possible. There is a rectangular hole (of the film size) in the center of the mica sheet, which is (almost) only gateway for evaporated species to come through for deposition. A smooth graphite block is kept on the substrate with heater arrangement. There is a hole for thermocouple in this graphite block, which is further connected to the temperature controller in order to maintain the required temperature of the substrate. The temperature of the substrate is controlled by a thermocouple attached with temperature controller along with relay. The switches attached with relay keeps ON and OFF the heater accordingly to maintain the substrate at required temperature.

2.3.6 The Selection of Substrates

There is a wide range of substrates that can be used according to the requirements of application or/and experimental conditions. The properties of deposited thin film also depend upon the substrate. To fabricate a good film, substrate must have a list of the properties approaching to an ideal substrate, although it is not possible. The desired properties in an ideal substrate may be formulated as in Table 2.1

Table 2.1 Properties of an ideal substrate.

Desired properties	Reasons
1 Mechanical strength	1 Prevents breakage
2 Atomically smooth surface	2 Provides film uniformity
3 No porosity	3 Prevents excessive out gassing
4 High thermal conductivity	4 Prevents heating of circuit components
5 Matching of thermal coefficient of expansion to that of deposited film	5 Prevents film stresses
6 Resistive to thermal shock	6 Prevents damage during processing
7 High electrical resistance	7 Provides insulation of circuit components
8 Thermal stability	8 Permits heating during processing
9 Chemical stability	9 Permits the unlimited use of process reagents
10 Low cost	10 Permits commercial application

In our case, the glasses used as substrate were selected to be of high transparency in the range required for optical studies. Micro slides and corning 7059 glass were used as a substrate in our experiment during fabrication of CdS thin films.

2.3.7 Substrate Cleaning

Cleanliness of the substrate is necessary for the better adhesion and constancy of film properties. To get absolutely cleaned and uncontaminated surfaces, is only possible in the case of surface of single crystal obtained in vacuum but it may not be possible in other cases. However it is not always necessary to get such an ideal conditions of cleanliness because we often deal with the removal of only detrimental contaminants. The option of different cleaning techniques depends on the type of the substrate, nature of contaminants and the degree of the cleanliness we need. Residues from manufacturing and packaging, oil, fingerprints and airborne particulate matter are examples of commonly encountered contaminants [13].

In general, the minimum requirement is to make the substrate surface cleaned enough that contaminants do not interfere with the adhesion of a vacuum deposited film. Cleaning involves the breaking of adsorption bonds between the substrate and the contaminants without damaging the substrate surface itself. The recommended procedure for cleaning the surfaces is; application of ultrasound radiation in solution of ionic detergent, through rinsing in deionized distilled water, degreasing in vapor of alcohol and then finally drying with stream of dry nitrogen. An efficient and commonly used technique for cleaning is ion bombardment [14]. In our case, first we removed the gross contamination mechanically i.e rubbing the substrate with cotton swabs by using solvent I.P.A (iso propyle alcohol). Then we suspended the substrates in an ultrasonically agitated detergent (I.P.A) solution at *60* ^{o}C for *60* minutes and then we let it dry in a closed clean glass dish/desiccators.

2.4 Experimental Procedure

2.4.1 Deposition

CdS thin films were deposited first on soda lime and corning glass substrates. The deposition of CdS thin films by the CSS technique is based on the following reversible dissociation of CdS at high temperature:

$$2CdS_{(s)} \Leftrightarrow 2Cd_{(g)} + S_{2(g)}$$

A very small distance of about 5 mm separates a CdS source and a substrate. The source is maintained at a higher temperature than the substrate. At a high temperature, the source CdS dissociates into its constituent elements (Cd and S), and then they recombine on the substrate surface, which is at a lower temperature.

The CSS system used in our experiment is shown schematically in Fig 2.1. The source material (CdS 99.999% purity) was placed in a graphite boat. The substrate was first cleaned with IPA bath in an ultrasonic cleaner at $60\ ^{o}$C for *60* minutes and then cleaned by lint free tissue with the help of tweezer and finger cots to avoid fingerprints on glass. It was then kept in the glass chamber (desiccator) for drying. The substrate was then supported by the cast (graphite) and kept in a close proximity to the source material. The vacuum chamber was then closed and allowed to evacuate by a rotary vane pump. The chamber was kept for evacuation for 1 hr each time and vacuum reaches approximately 2×10^{-3} mbar depending on the source temperature. The source and substrates could be maintained at the desired temperature as they were heated and controlled separately. Two K-type thermocouples were used to monitor the temperature of the source and the substrate during the evaporation process. The temperatures of the source and substrate were maintained at *500*℃ and *400*℃, respectively. The deposition time was different varying from 5min to 18min to attain films of different thickness. These parameters yield stoichiometric CdS thin film. The film was then kept at substrate temperature until the temperature of source became lower than the substrate temperature after that the substrate heater was switched off to allow cooling to ~ *60*℃ before opening the vacuum chamber. By using the automatic temperature controller for heating the

source and substrate, the quality of the film is quite improved. After the deposition of CdS (99.999% purity), these samples (films) were annealed at *450*℃ and 10^{-2}mbar for 30min. After deposition and annealing, the films were removed from the chamber and different properties were studied.

2.4.2 Characterization of CdS Thin Films

The surface morphology, grain sizes and surface roughness were examined with the help of scanning electron microscopy (SEM) and Atomic Force Microscopy (AFM). The compositions of the samples were determined by the energy dispersive X-ray spectroscopy (EDX). The structure of the films was studied by X-ray diffraction (XRD) technique. Resistivity and conductivity of samples were measured (van der Pauw method) with Hall Measurement apparatus at *77*K, *300*K and high temperature. Optical transmission spectra were recorded with Perkin-Elmer, Lambda900, UV-VIS-NIR spectrophotometer.

2.4.3 Doping of Silver (Ag)

To improve the electrical Properties of CdS thin films, we doped these samples with Silver (Ag) by using ion-exchange solution method. We dipped the samples for different time ranges from 1min to 30min in the solution of $AgNo_3$ and distilled water having ratio of *0.1*g: *100*ml respectively. After that we let it dry in a closed clean glass dish/desiccators. All the samples were annealed at *400* ^{o}C at a pressure of $\sim 10^{-2}$ mbar for *30* min, for diffusion of Ag into the film.

2.4.4 Characterization of Ag-doped CdS Thin Films

After doping of Silver (Ag), we characterized again the physical properties of these samples and studied the variation in the properties after and before doping.

Reference

1. K. L. Chopra, Thin Film Phenomena, McGraw-Hill, New York (1969).
2. R.W. Berry, P. M. Hall, M. T. Harris, Thin Film Technology, D. V. Nostrand Company, Inc (1968).
3. Ullmann's Encyclopedia of industrial Chemistry, A26 VCH (1995).
4. J. Britt, C. Ferekids, Appl. Phys. Lett. **62** (1993) 285.
5. Y. Kashiwaba, H. Kirita, H. Abe and T. Lkeda, Jpn. J. Appl. Phys. **29** (1990) 1733.
6. I. Broser, Ch. Fricke, B. Lummer, H. Peris and A. Hoffman, J. Crys. Growth, **117** (1992) 788.
7. J. Britt, C. Ferekids, Appl. Phys. Lett. **62** (1993) 285.
8. A. Haque, A. E. Dixon and D. E. Brodic, Can. J. Appl. Phys. **65** (1987)1015.
9. Y. Kashiwaba, H. Kirita, H. Abe and T. Lkeda, Jpn. J. Appl. Phys. **29** (1990) 1733.
10. I. Broser, Ch. Fricke, B. Lummer, H. Peris and A. Hoffman, J. Crys. Growth, **117** (1992) 788.
11. N. V. Lugueva, S. M. Luguev and A. A. Guseinov, Inorganic Materials **40** (2004) 122.
12. K. Seshan, Hand Book Of Thin-Film Deposition Processes And Techniques, Intel Corporation, California (2000).
13. L. I. Maissel, R. G. Lang, Handbook of Thin Film Technology, McGraw Hill, Inc. (1970).
14. L. Eckertová, Physics of Thin Films, Plenum Press, New York, (1977).

Chapter 3
Characterization Techniques

To prepare defect free thin films by any method is very difficult. Such prepared thin films generally contain impurities, defects, unwanted phases and in-homogeneities. To study these physical effects and morphologies of thin films, we use different characterization techniques. "Characterization" has different meanings in different contexts but in the following discussion it includes physical explanation of film. To study the structural and surface morphologies, thin films are characterized by X-ray diffraction (XRD) technique, scanning electron microscopy (SEM), energy dispersive X-ray (EDX) and atomic force microscopy (AFM). Electrical properties are examined with the help of Hall measurement apparatus. To discuss optical properties, films are characterized by spectrophotometer. A short description of above characterization techniques is given here.

3.1 Structural Characterization

3.1.1 X-Ray Diffraction

X-ray diffraction (XRD) technique is a method of determining the arrangement of atoms within a crystal, in which a beam of X-rays strikes a crystal and diffracts into many specific directions. From the intensities and the angles of these diffracted beams we can get some specific information about our specimen. X-ray diffraction technique is the most suitable, powerful, non-destructive and general method for structure analysis of thin films. It provides information on structures, phases and preferred crystal orientations (texture) [1-2]. Some other structural parameters can also be calculated such as average grain size, particle size, crystallinity, strain and crystal defects. Crystals are regular arrays of atoms, and X-rays are electromagnetic radiation with typical photon energies in the range of *100*eV – *100*KeV. X-rays are used to produce the diffraction pattern because their wavelength 'λ' is typically the same order of magnitude (1-100Å) as the spacing 'd' between planes in the crystals or comparable to size of atoms. The energetic X-rays can penetrate deep into the materials so it also provides information about the bulk structure.

X-ray waves are scattered by atoms, primarily through the atoms' electrons. Just as an ocean wave striking a lighthouse produces secondary circular waves originating from the lighthouse, so an X-ray striking an electron produces secondary spherical waves originating from the electron. This phenomenon is known as elastic scattering, and the electron (or light house) is known as the scatterer. A regular array of scatterers produces a regular array of spherical waves. These waves cancel and add up each other at different conditions which are described by Bragg's law. For a given set of lattice plane with inter-planer distance of 'd', condition for diffraction (peak) to occur can be simply written as:

$$2d \, Sin\, \theta = n\lambda \qquad \text{.....(3.1)}$$

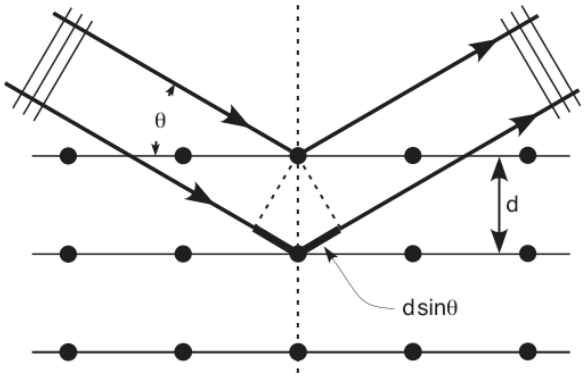

Where

d = Normal spacing between adjacent plane,

θ = Angle between the incident wave and reflected plane.

n = Order of reflection

λ = Wavelength of X-ray

This is known as Bragg's law, after W.L Bragg, who first proposed it.

X-ray peaks of diffractions are produced by constructive interference of monochromatic beam scattered from each set of lattice planes of specific angles. The peak intensities are concerned with the atomic density within the lattice planes. Consequently, the X-ray diffraction pattern is the fingerprint of periodic atomic arrangements in a given specimen. In case of rotating crystal method, specimen is mounted at some specific direction and it

rotates such that particular sets of lattice planes make correct Bragg angle for reflection when X-ray beam falls on it [3].

Improvement in intense micro-focus X-ray source and availability of specific monochromators and advanced detection methods of X-rays has made it possible to apply this technique to characterize films as thin as *100*Å [4]. By Comparison of diffraction patterns obtained with the standard ASTM cards and with its analysis we can derive different information about our specimen such that phases, lattice parameters and preferred orientations in film [1]. From diffraction line width, average grain size of film can be estimated [3,4]. From peak broadening, we can calculate crystallite size, which is given by the mathematical relation [3,4]:

$$d = 0.9\,\lambda / (D \cos\theta) \qquad (3.2)$$

Where

D = Angular width at half maximum intensity,

θ = Bragg angle,

λ = Wavelength of X-ray

Here one point should be noted that, a grain can contain more than one crystallite. So the parameter on which the crystallite depends and grains also.

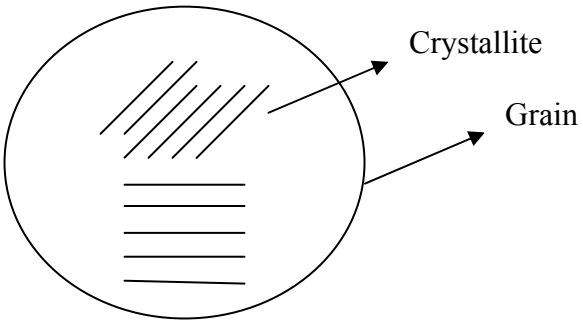

It is accepted [5,6] that a crystallite size is the coherent diffraction domain in the film and that the grains are larger than crystallites and are formed by several of them. Crystallite size is usually measured from X-ray diffraction patterns [6-10] and grain size by other experimental techniques like transmission electron microscopy (TEM), scanning electron microscopy (SEM), atomic force microscopy (AFM) etc depending on the type and characteristics of the material [5].

In our work, Cu Kα (λ = *1.5418* Å) radiations were used for the structural characterization. These characterizations were done with the help of XRD machine available at our department, School of Chemical & Materials Engg (SCME), NUST.

3.2 Surface and Compositional Analysis

3.2.1 Scanning Electron Microscopy

Traditionally, the optical microscope comes in mind for small scale materials investigation. For the detailed materials characterization, optical microscope has been replaced by instruments having better spatial resolution and depth of focus.

The scanning electron microscope (SEM) provides investigator with highly magnified image of surface of a specimen that is very similar to what one would expect if one could actually "see" the surface visually [11].

The scanning electron microscope (SEM) is an apparatus designed primarily for investigating the surfaces of solids at higher magnifications. Images formed in SEM follow a quite different mechanism from that in an optical microscope, where objective lenses are used. Instead of objective lens, here images are built point by point in a similar way as formed in television display. In SEM, a beam of electrons is produced at the top of the microscope by an electron gun. The electron beam is focused (in vacuum) into a fine probe with the help of electromagnetic fields and lenses. This focused electrons beam hits the specimen which is to be investigated. Once the beam hits the sample, different kind of interactions can occur which result into the emission of electrons (of different energies) or/and photons from (or through) the surface of sample.

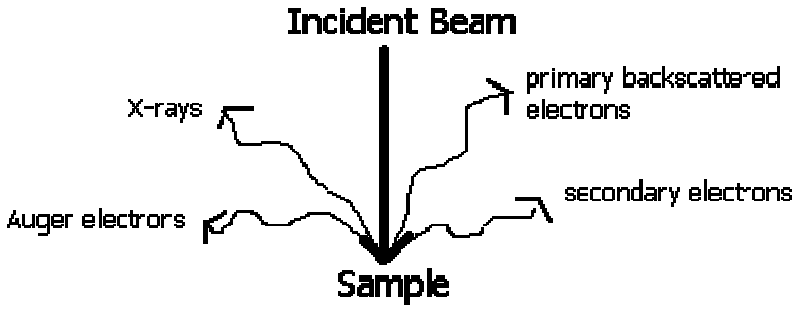

A reasonable fraction of the emitted electrons are collected by appropriate detectors and then output can be used to modulate the brightness of a cathode ray tube (CRT) display.

Whose x- and y-inputs are driven in synchronism with the x-y voltages rastering the electron beam. To build up the complete image, the electron beam in the microscope is scanned over an area on the specimen surface (the pattern of scan is called a raster) while a beam in the CRT display is scanned over a geometrically similar raster. Thus every point that the beam hits the sample is mapped directly on the corresponding point on the CRT display screen. Darker area of the image on CRT display corresponds to low intensity of signal which means very few electrons are emitted. Brighter area of image corresponds to the increased intensity of signal which means more numbers of electrons are emitted. Thus the image on the CRT is a map of the intensities of the electron emission from the specimen surface.

The principle images produced in the SEM are of three types: secondary electron images, backscattered electron images, and elemental X-ray maps [12]. Secondary and backscattered electrons are conventionally separated according to their energies. The higher the atomic number of a material, the more likely it is that backscattering will occur. Thus as a beam passes from a low-Z (atomic number) to a high-Z area, the signal due to backscattering, consequently the image brightness will increase. There is a built in contrast caused by elemental differences.

Scanning electron microscope (SEM) utilizes an electron beam to produce a magnified image of the sample. Its schematic diagram is shown in Fig.3.1. It consists of the following three major sections [13,14]:

1. Electron-optical column
2. Vacuum system
3. Electronics and display

In currently available SEMs, the electron beam energy can range from few hundred eV up to 30 keV. There are several possible interactions between electrons and samples which plays an important role in image formation and for chemical analysis. The magnification is given simply by the ratio of side lengths of display and specimen rasters, and is normally variable from about *20*× to *100000*×. The resolution can be defined in terms of ability to see two closely situated objects apart.

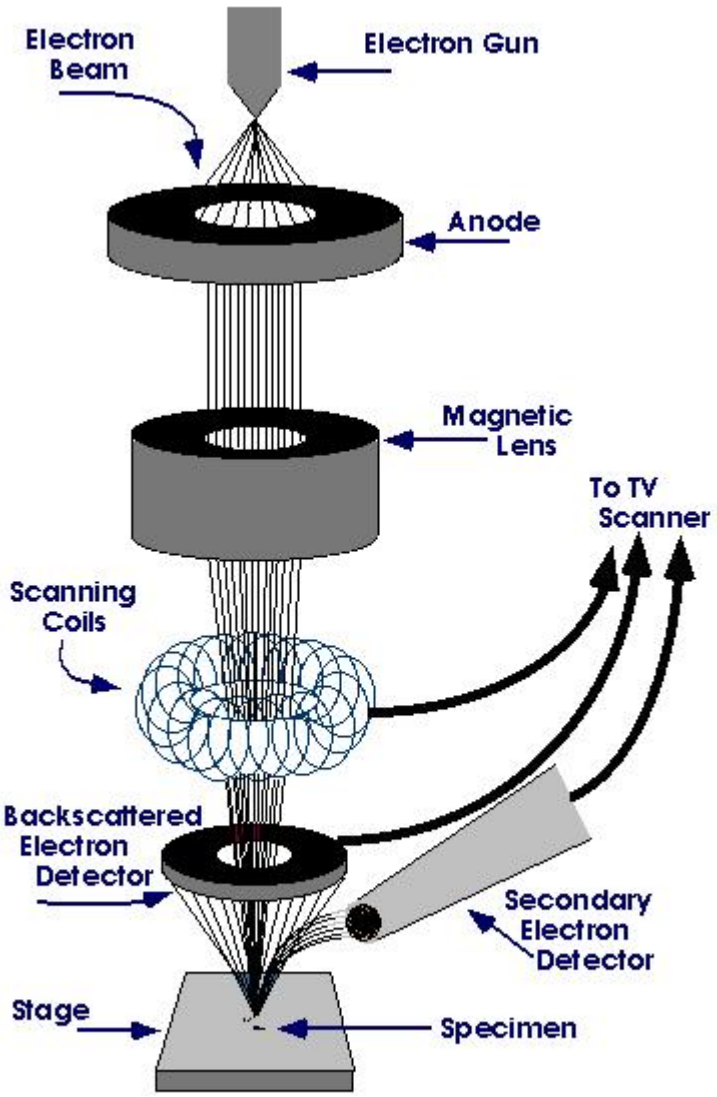

Fig3.1 Schematic diagram of Scanning Electron Microscope (SEM).

It is more important quantity for any microscope. In current high performance instruments, this quantity can be as small as 5nm. However, the resolution in SEM depends critically upon the nature of the sample and mode of operation of instrument [15].

3.2.2 EDX Analysis

X-rays which are also generated by the interaction of (primary) electrons with the specimen may also be detected in a SEM equipped for energy

dispersive X-ray spectroscopy (EDX or EDS) or wavelength dispersive X-ray spectroscopy (WDS).

For identification of elemental composition, energy dispersive X-ray (EDX) spectroscopy is used. In scanning electron microscope (SEM), EDX analysis system works as an integrated feature [16]. Inside the scanning electron microscope, the specimen is bombarded with an electron beam for EDX analysis. In the process, some of specimen's electrons knocked off when they collide with bombarding electrons. Higher energy electron from an outer shell occupies the vacant position of ejected inner shell electron. In this phenomenon, outer electron emits some energy in form of X-ray. This amount of energy depends upon those shells, in which give and take process of electrons being occurred. Furthermore, different elements emit X-rays of unique energy during this process. Thus atoms can be identified present in the specimen by measuring the amount of energy of X-rays emitted by specimen during this process. In EDX analysis, we get EDX spectrum as an output. EDX spectrum gives information that how frequently an X-ray is received for each energy level. In EDX spectrum, those peaks, corresponding to the energy levels, are displayed normally for which the most X-rays had been received. Each peak represents a particular atom which corresponds to a single element. Intensity of peak in spectrum shows the concentration of that element in specimen.

3.2.3 Atomic Force Microscopy

The atomic force microscope (AFM) provides an investigator with highly magnified image of surface of a specimen that is very similar to what one would expect if one could actually "feel" the surface.

The atomic force microscope (AFM) is a powerful characterization tool for investigating surfaces, in which a sharp probe is used to scan the surface of a sample. Instead of using an electrical signal, like in scanning electron microscopy (SEM), the AFM works on the principle of sensing forces between the atoms in the tip and in the sample [17]. The major parts of AFM are thin cantilever with very sharp (*50* nm to *10* nm in radius) probing tip, a optical system to measure deflection of the cantilever and 3D piezo-electric scanner. The probe of the AFM is a flexible cantilever—think of a diminutive diving board—with a tip attached to its underside. Combination of the surface forces (attractive and repulsive) affects the tip when tip is brought into the contact with the surface or in its proximity, or

is tapping the surface. Bending and torsion occurs in cantilever because of those forces and is continuously measured via the deflection of reflected laser beam. For the scanning of predetermined area of the surface, 3D scanner moves the sample or, in alternative designs, the cantilever, in 3 dimensions. Force between them is monitored as the tip scans the sample. Cantilever moves up and down to keep the force constant. The vertical motion of the cantilever, which represents the hills and valleys of the sample's surface, is measured by a device usually a reflected laser beam. This vertical image is translated by computer into an image.

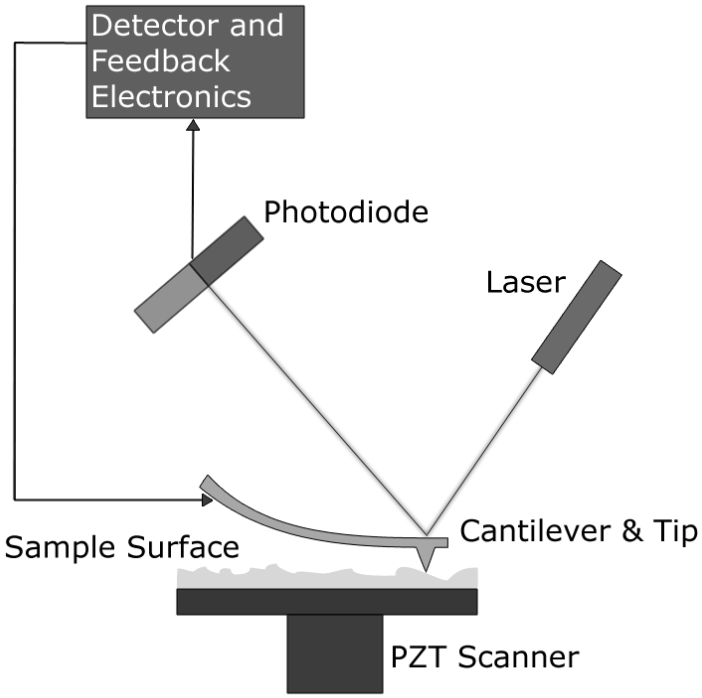

Fig 3.2 Block diagram of AFM operation.

An inter-atomic, van der Waals force is most commonly associated with AFM. Distance between the tip and the sample corresponds to the degree of Van Der Walls force which is shown in Figure 3.3 [18].

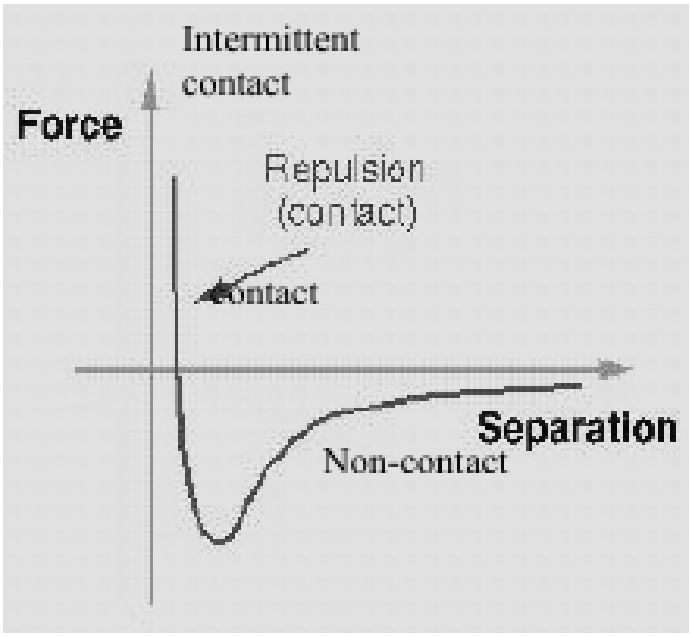

Fig. 3.3 Force distance curve.

The distance regimes are shown in Figure 3.3: (1) contact regime; (2) non-contact regime. The cantilever is held at a few angstroms from the sample's surface, in contact regime, and the inter-atomic force between the sample and cantilever is repulsive. The cantilever is held of the orders of tens to hundreds of angstroms from the sample's surface, in non-contact regime, and the inter-atomic force between the cantilever and sample is attractive (largely a result of the long-range van der Waals interactions).

The AFM can be operated in tapping, non-contact and contact mode depending upon the application. Tapping mode has been used in our work.

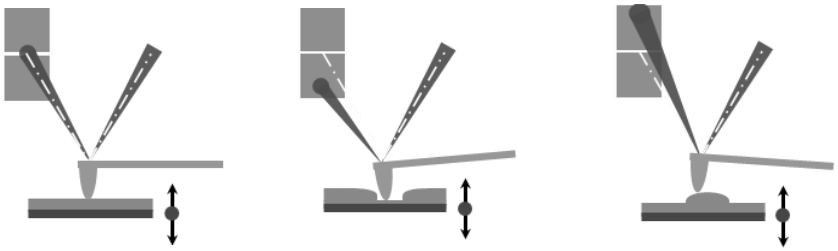

In addition to gathering information about the topography of a sample, AFM can measure the friction between the tip and the sample, and the degree of roughness of sample. In our case, we used AFM available at school of chemical and materials engineering, for the characterization of our samples.

3.3 Optical Characterization

To study the optical properties of thin films are very significant for various application points of view, including interference devices, as well as optoelectronics, solar cells, integrated optics, optical sensor technology and micro- electronics. Regarding characterization tools different methods are being used such as spectrophotometric, interferometric, ellipsometric, photothermal, and combined methods as well.

Transmission of a film is the only property, which is obtained directly from the film. The rest are inferred from the transmission plots. Transmission can be recorded by using an instrument known as spectrophotometer, a short description of which is described below.

3.3.1 The Spectrophotometer

Instruments that are used to measure the optical transmission or reflection characteristics of a sample over a range of wavelengths are termed as 'Spectrophotometers'. All spectrophotometers contain four elements [16]:

- A source of radiation;
- An optical system, or monochromator, to isolate a narrow band of wavelengths from the whole spectrum emitted by the source;
- The sample (and its cell if it is liquid or gaseous);
- A detector of radiation and its auxiliary equipment.

Spectrophotometer may be either 'single beam' or double beam. In a single beam spectrophotometer the light beam takes a single fixed path and the measurements are affected by taking measurements with and without the sample present. In the double beam the light passes alternately through the sample and the reference cuvets.

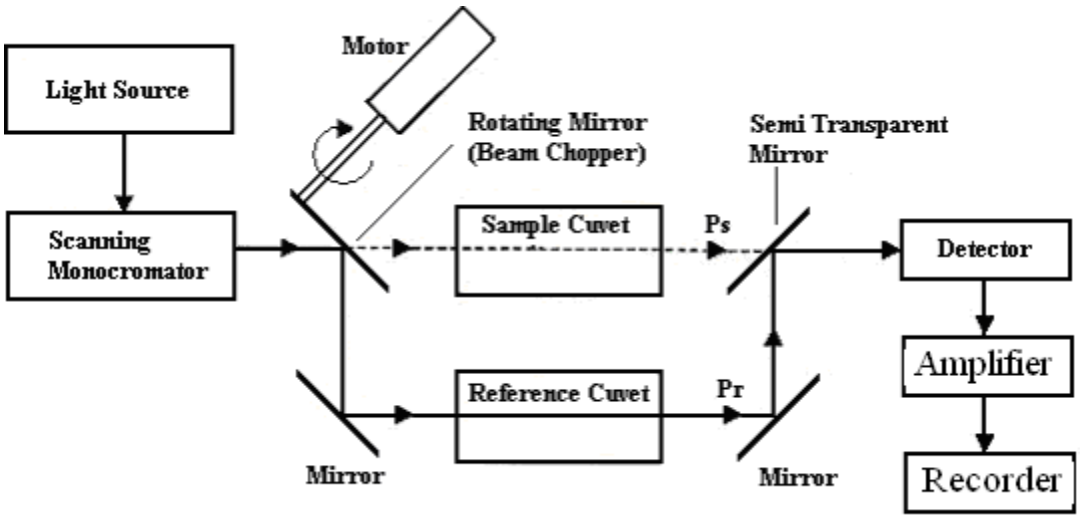

Fig. 3.2 Schematic diagram of a double beam scanning spectrophotometer.

This is accomplished by a motor, which rotates the mirror into and out of the light path. When the chopper is not diverting the beam, the light passes through the sample, and the detector measures the radiant power Ps. When the chopper diverts the beam through the reference cuvet, the detector measures P_r as shown in Fig.3.2. The beam is chopped several times per second, and the circuitry automatically compares P_r and P_s to obtain absorbance using equation [19],

$$A = \log \frac{P_s}{P_r} \quad \text{..... .....} \quad (3.3)$$

Since spectrophotometer results are nearly used in extension calculations and much data can easily be collected. Spectrometers are some times equipped with microprocessors and are commonly used to control a variety of automatic functions, e.g. the wavelength–scanning mechanism, automatic sample changing, slit width, filter and lamp selection.

3.3.2 Determination of Optical Parameters of Thin Films

The optical behavior of thin films deals primarily with optical transmission, absorption and reflection properties of thin films. From transmission, reflection and interferometric properties, it is possible to determine other optical parameters [4]. Many methods have been proposed to determine the other optical parameters from the optical transmission data [20-27]. This is because of the simplicity of calibration of the

spectrophotometer, which yields accurate experimental rsults. One of the simplest method was introduced by Sawnepoel [20], which used the transmission envelope to solve the equations for the values of thickness and referective index. However, including thickness variation in his formula [21] required a numerical solution for every data point. For the measurement of optical parameters, we proceed as follows:

Let us consider a thin film is deposited on a transparent substrate, and then practical situation will be such as shown in Fig. 3.3

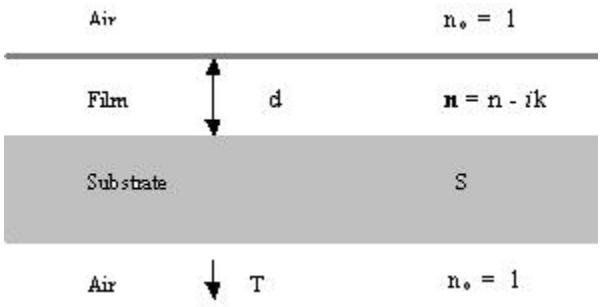

Fig.3.3 System of an absorbing thin film on a transparent substrate

The film has thickness 'd' and complex refractive index $\boldsymbol{n} = n\text{-}ik$, where '$n$' is the refractive index and k is the extinction coefficient which can be expressed in terms of the absorption coefficient 'α' as $k = \alpha\lambda/4\pi$.The transparent substrate has a thickness several orders of magnitude larger than'd' and has refractive index *'S'* and absorption coefficient $\alpha_s = 0$. The system is surrounded by air with refractive index n_o=1. The optical transmission 'T' for normal incidence is given by Swanepoel [20]:

$$T = \frac{AX}{B - CX\cos\phi + DX^2} \quad \text{.....(3.4)}$$

Where $A = 16n^2S,$

$$B = (n+1)^3(n+S^2),$$

$$C = 2(n^2-1)(n^2-S^2),$$

$$D = (n-1)^3(n-S^2),$$

$$\phi = \frac{4\pi.nd}{\lambda},$$

$$X = e^{-\alpha.d}$$

By using this form, interference envelop consisting of the functions (maxima T_M and minima T_m) that pass through the extreme points in the spectrum ($Cos\phi = \pm 1$) are defined as [28],

$$T_M = \frac{AX}{B - CX + DX^2} \quad \ldots\ldots\ldots\ldots\ldots\ldots\ldots\ldots\ldots\ldots\ldots\ldots(3.5)$$

And

$$T_m = \frac{AX}{B + CX + DX^2} \quad \ldots\ldots\ldots\ldots\ldots\ldots\ldots\ldots\ldots\ldots\ldots\ldots(3.6)$$

The upper function T_M passes through the maxima of the spectrum and T_m through the minima.

The above equations may be written as:

$$\frac{1}{T_M} = \frac{B - CX + DX^2}{AX} \quad \ldots\ldots\ldots\ldots\ldots\ldots\ldots\ldots\ldots\ldots\ldots (3.7)$$

$$\frac{1}{T_m} = \frac{B + CX + DX^2}{AX} \quad \ldots\ldots\ldots\ldots\ldots\ldots\ldots\ldots\ldots\ldots\ldots\ldots(3.8)$$

Here we assume that $n_M = n_m$ and $\alpha_M = \alpha_m$

$$\frac{1}{T_m} - \frac{1}{T_M} = \frac{2C}{A},$$

$$\frac{1}{T_m} - \frac{1}{T_M} = \frac{4(n^2 - 1)(n^2 - S^2)}{16n^2 S},$$

$$\frac{1}{T_m} - \frac{1}{T_M} = \frac{4(n^2 - 1)(n^2 - S^2)}{16n^2 S},$$

$$\frac{1}{T_m} - \frac{1}{T_M} = \frac{n^4 - n^2 S^2 - n^2 + S^2}{4n^2 S} \quad \ldots\ldots\ldots\ldots\ldots\ldots(3.9)$$

Let $n^2 = N$

$$\frac{1}{T_m} - \frac{1}{T_M} = \frac{N^2 - NS^2 - N + S^2}{4NS}, \quad \ldots\ldots\ldots\ldots\ldots(3.10)$$

Again let us assume that

$$V = \frac{1}{T_m} - \frac{1}{T_M}$$

So equation (3.10) becomes

$$4NSV = N^2 - NS^2 - N + S^2,$$

$$N^2 - NS^2 - 4NSV - N + S^2 = 0,$$

$$N^2 - N(S^2 + 4SV + 1) + S^2 = 0, \quad \text{..... (3.11)}$$

Let $S^2 + 4SV + 1 = \phi,$

So equation (3.11) becomes

$$N^2 - \phi N + S^2 = 0,$$

And the solution of this equation will be;

$$N = \frac{\phi \pm \sqrt{\phi^2 - 4S^2}}{2}$$

Now using the values of $\phi \,\&\, V$ we have

$$N = \frac{[S^2 + 4S(\frac{1}{T_m} - \frac{1}{T_M}) + 1] \pm \sqrt{[S^2 + 4S(\frac{1}{T_m} - \frac{1}{T_M}) + 1]^2 - 4S^2}}{2} \quad \text{.....(3.12)}$$

Where $N = n^2$ or $n = \sqrt{N}$

Thus value of '*n*' can be calculated by using the above formula.

For the calculation of '*d*', thickness of the film, we proceed as follows;

As $\phi = \frac{4\pi.nd}{\lambda},$

So $Cos\phi = Cos(\frac{4\pi.nd}{\lambda}),$

For maximum value

$$Cos\phi = 1,$$

$$\frac{4\pi.nd}{\lambda_M} = 2\pi.m,$$

For minimum value

$$\frac{4\pi.nd}{\lambda_m} = (2m+1)\pi,$$

Therefore

$$\frac{4nd}{\lambda_M} = 2m, \ldots\ldots (3.13)$$

$$\frac{4nd}{\lambda_m} = (2m+1), \ldots\ldots (3.14)$$

By using equations (3.13) and (3.14) we obtain

$$\frac{4nd}{\lambda_m} = \frac{4nd}{\lambda_M} + 1,$$

$$4nd\lambda_M = 4nd\lambda_m + \lambda_m\lambda_M,$$

$$4nd(\lambda_M - \lambda_m) = \lambda_m\lambda_M,$$

$$4nd = \frac{\lambda_m\lambda_M}{\lambda_M - \lambda_m},$$

$$d = \frac{1}{4n}\left[\frac{\lambda_m\lambda_M}{\lambda_M - \lambda_m}\right], \ldots\ldots (3.15)$$

The values of '*n*' and '*d*' , calculated from equations(3.12) and (3.15) are used as initial least square fitting parameters for equation(3.4) [29]. For good fitting, approximation model for '*n*' and 'α ' should be used. While for the calculation of absorption co-efficient,'α' near the absorption edge (required for calculation of band gap) following procedure will be used:

$$T = \frac{AX}{B - CXCos\phi + DX^2} \quad ,$$

For $CCos\phi = C_1$,

Therefore $$T = \frac{AX}{B - C_1X + DX^2}$$

$$TB - TC_1X + TDX^2 = AX$$

$$TDX^2 - (A + TC_1)X + TB = 0$$

$$DX^2 - \left(\frac{A}{T} + C_1\right)X + B = 0$$

$$X = \frac{\left(\frac{A}{T} + C_1\right) \pm \sqrt{\left(\frac{A}{T} + C_1\right)^2 - 4BD}}{2D} \ldots\ldots (3.16)$$

In equation (3.16), +ve sign in case of $n > S$ gives $X > 1$, while –ve sign gives $X < 1$ which is physically accepted due to the reason given below,

$$X = e^{-\alpha.d}$$

$$\ln X = -\alpha.d$$

$$\alpha = -\frac{1}{d}[\ln X] \quad \text{.....(3.17)}$$

If $X > 1$, α is –ve, which is non-physical.

So the –ve sign in equation (3.16) is the physically accepted solution.

Therefore, exact solution of equation (3.4) for X is,

$$X = \frac{(\frac{A}{T} + C_1) - \sqrt{(\frac{A}{T} + C_1)^2 - 4BD}}{2D} \quad \text{.....(3.18)}$$

Where all the constants have been already defined.

The optical absorption edge can be analyzed by the following relation [30-32] :

$$\alpha h\nu = A(h\nu - E_g)^m \quad \text{.....(3.19)}$$

Where A is edge parameter, representing the film quality, which is calculated from the linear part of this relation, E_g is the optical energy band gap of the sample and 'm' determines the type of transition. The parameter 'm' is a constant, which is different for various transitions, indicated by the values of ½, 2, 3/2, 3 for allowed direct, allowed indirect, forbidden direct and forbidden indirect transitions respectively.

The absorption edge is determined by extrapolating the steep portion of α vs λ plots on wavelength. The energy gap is obtained by means of extrapolating the square of the absorption coefficient (α^2) versus incident photon energy ($h\nu$) for direct transition. Once α is known, the extinction coefficient *'k'* can be calculated from the equation:

$$k = \frac{\alpha\lambda}{4\pi} \quad \text{.....(3.20)}$$

This completes the calculation of the optical parameters.

3.4 Electrical Characterization

The Investigation of electrical properties in semiconductor materials has great importance because of their dependent behavior on impurities and defects in crystals. It becomes more interesting when we work in regime of thin films. In thin films, surface properties become significant which effect on conductivity and other parameters related to the electrical regime. We can say that surface properties and effects in semiconductors especially in thin films have great influence on electrical properties. To re-fabricate a sample of thin film under same conditions and having exact parameters is generally very difficult job. So as an outcome, the diversity in the results reported by different authors on same (semiconductor thin films) materials have been greater than that for metals. In electrical characterization, we have different parameters to be focused on it but in general we do concern with resistivity, mobility, charge carriers and doping type etc. Different methods can be used to find out electrical parameters. Van Der Pauw Hall measurements are well known and easy method to calculate the different electrical parameters of a semiconductor material.

3.4.1 The Hall Effect

The Hall Effect was discovered in 1874, by E. H. Hall which is a standard tool to study the mobile carrier density and the type (sign) of the charge carriers in solids. In this experiment, an electric current is passed through the semiconductor block while a magnetic field **B** is applied perpendicular to the current as shown in Figure 3.4. Because of this setup a field is generated called as Hall voltage which is recorded perpendicular to the direction of current flow.

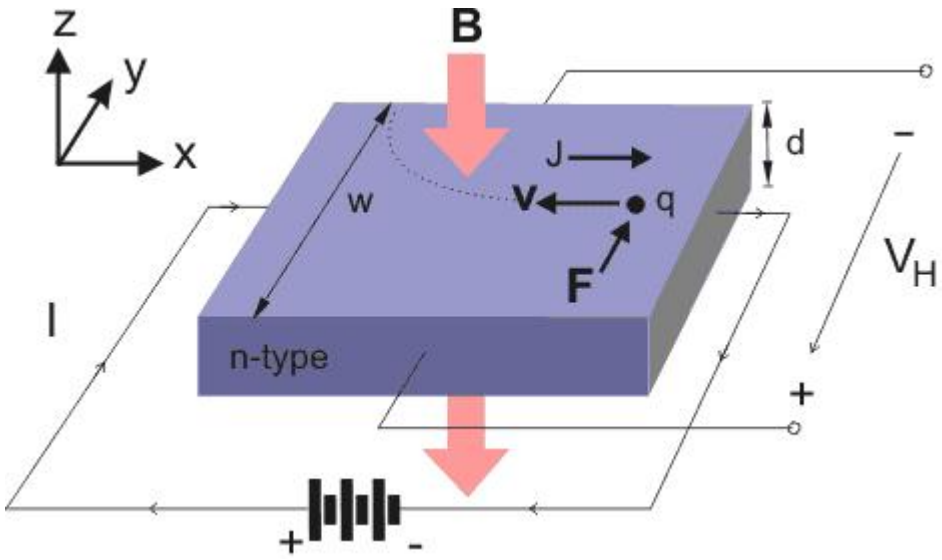

Fig. 3.4 Schematic diagram of the Hall Effect. An n-type semiconductor with a current applied across and magnetic field perpendicular to the current exhibits a potential difference perpendicular to both the current and the magnetic field, which is known as the Hall Effect.

Hall [33] showed that if a magnetic field is applied on a conductor, perpendicular to the current flowing in it, a potential difference will appear perpendicular to both magnetic field and current, which is called the Hall voltage.

The force bear by the moving charge carriers in a magnetic field is the Lorentz force.

$$F = q[E + (V \times B)] \quad \text{.....(3.21)}$$

F, V and B form a right-handed Cartesian co-ordinate system. Since V and B are arranged perpendicular to each other, the resultant force is also perpendicular to both V and B.

Hall voltage can be expressed mathematically such as:

$$V_H = \frac{JR_H B_Z}{t} \quad \text{.....(3.22)}$$

Where t is thickness of the sample and R_H is Hall constant. In case of electrons as majority carriers, Hall constant is negative and in case of holes it is positive.

$$R_H = \frac{p\mu_e^2 - n\mu_h^2}{q(n\mu_e + p\mu_h)} \quad \text{.....(3.23)}$$

Where μ_e , μ_h are mobility of electrons and holes respectively.

With a measurement of the Hall coefficient the mobility can be found.

$$\mu = \frac{R_H}{\rho} \quad \text{.....(3.24)}$$

Where ρ is the resistivity of sample which is most commonly obtained using the Van Der Pauw technique. Van Der Pauw technique is explained as below.

3.4.2 Van Der Pauw Method

To measure the resistivity of a thin, arbitrary-shaped sample with four Ohmic contacts Van der Pauw technique can be used. By using Van der Pauw method sheet resistance R_s of the sample is measured [34]. According to Van der Pauw demonstrated that there are two characteristics resistances, R_A and R_B, associated with the four terminals.

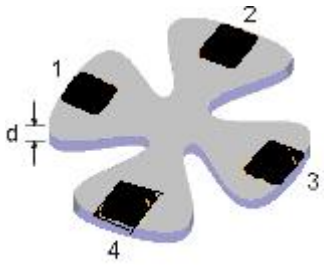

$$R_A = \frac{V_{43}}{I_{12}} \quad , \qquad R_B = \frac{V_{14}}{I_{23}}$$

Voltage measured across terminals 4 and 3 is V_{43}, and I_{12} is the current measure across terminals 1 and 2. Voltage measured across terminals 1 and 4 is V_{14} and I_{23} is the current measured across terminals 2 and 3. R_A and R_B relate to the sheet resistance through the Van-der Pauw equation.

$$\exp(-\pi \frac{R_A}{R_S}) + \exp(-\pi \frac{R_B}{R_S}) = 1 \quad \text{.....(3.25)}$$

Which can be solved numerically for R_s. The resistivity can then be calculated using equation:

$$\rho = R_S t \quad \text{.....(3.26)}$$

By measuring Hall voltage $V_{H,}$ in van der Pauw technique sheet carrier density n_s is determined. By keeping current and perpendicular magnetic field B constant, series of voltage is measured which corresponds to Hall voltage measurements. The sheet carrier density n_s can be calculated via

$$n_S = \frac{IB}{q|V_H|} \quad \text{.....(3.27)}$$

To avoid the errors, quality and size of ohmic contacts, accurate thickness and uniformity of sample is very important.

In our case, we used Ecopia HMS3000 Hall measurement system in our lab to perform all experiments for the calculation of resistivity, mobility and carrier concentration.

Reference

1. K. L. Chopra and S. R. Das, Thin Film Solar Cells, Plenum Press, New York, (1983).
2. D. K. Schroder, Semiconductor Materials and Device Characterization (2nd Ed.), John Wiley & Sons, Inc. (1998).
3. B. D. Cullity, Element of X-ray Diffraction, Addison-Wesely Publishing Company, Inc. (1978).
4. K. L. Chopra, Thin Film Phenomena, McGraw-Hill, New York (1969).
5. J. R. Ares, A. Pascual, I. J. Ferrer, C. Sa ´nchez. Thin Solid Films (2005) 480.
6. M. L. Lavcevic, A. Turkovic, Scr. Mater. **46** (2002) 501.
7. H. Q. Li, F. Ebrahimi, Acta Mater. **51** (2003) 3905.
8. K. Okada, T. Nagashima, Y. Kameshima, A. Yasumori, Ceram. Int. **29** (2003) 533.
9. G. Xu, Y. W. Zhang, Ch. S. Liao, Ch. H. Yan, Solid State Ionics **166** (2004) 391.
10. E. Leite, M. I. B. Bernardi, E. Longo, J. A. Varela, C. A. Paskocimas, Thin Solid Films **449** (2004) 67.
11. C. R. Brundle and C. A. Evans, Jr. Materials Characterization Series, Reed Publishing Inc. USA, (1992).
12. J. I. Goldstien, D. E. Newbury, P. Echlin, D. C. Joy, C. Fiori, and E. Lifeshin. Scanning Electron Microscopy and X-Ray microanalysis, Plenum Press, New York (1981).
13. D. K. Schroder, Semiconductor Materials and Device Characterization (2nd Ed.), John Wiley & Sons, Inc. (1998).
14. G. Lawes, A. M. James, Scanning Electron Microscope and X-Ray Microanalysis, John Wiley & Sons, Chichester (1987).
15. D. K. Bowen and C. R. Hall, Microscopy of Materials, The Macmillian Press Ltd. New York (1975).
16. B. E. Noltingk, Instrumentation Ref. Book 2nd Edition, Butterworth Heinemann Ltd. **92** (1995).
17. G. Binnig, C. F. Quate, C. Gerber, Phys. Rev. Lett. **56**, (1986) 930.

18. R. Howland and L. Benatar, A practical guide to Scanning Probe Microscopy, (2000).
19. D. C. Harris, Quantitative Chemical Analysis, 3rd Edition, W. H. Freeman & Company, New York, Inc. (1991).
20. R. Swanepoel, Phys. E: Sci. Instrum. **16** (1983) 1214.
21 R. Swanepoel, Phys. E: Sci. Instrum., **17** (1984) 896.
22. J. I. Cisneros, Applied Optics **37** (1998) 5262.
23. J. Torres, J. I. Cisneros, F. Alvarez, Thin Solid Films Applied **289** (1996) 238.
24. K. F. Palmer and M. Z. Williams, Applied Optics **24** (1985)1788.
25. A. Bennouna, Y. Laaziz and M. A. Idrissi, Thin Solid Films **213** (1992) 55.
26. I. Chambouleyron, J. M. Martinez, Applied Optics **36** (1997) 8238.
27. M. Nowak, Thin Solid Films **254** (1995) 200.
28. A. K. S. Aqili, A. Maqsood, Z. Ali, Applied Surface Science **180** (2001) 73.
29. A. K. S. Aqili. A. Maqsood and Z. Ali, Appl. Surf. Sci. **191** (2002) 280.
30. N. Kenny, C. R. Kannewurf, D. H. Whitmore, J. Phy. Chem. Solids **27** (1966) 1237.
31. N. F. Mott, E. A. Davis, Electronic Process in Non-Crystalline Materials, Calendron Press, Oxford, (1979).
32. M. M. Abdel Aziz, E. G. El-Metwally, M. Fedel, H. H. Labib, Thin Solid Films **99** (2001) 386.
33. R. Hall, J. Sci. Intum, **44** (1967) 53.
34. V. Pauw**,** et al*,* Philips Research Reports **13** (1958) 1.

Chapter 4
Results and Discussion

Thin films of CdS can be fabricated by different techniques and being widely used in different optoelectronic devices due to favorable electrical and optical properties (paragraph 1.5.2). For wide range of application, thermally evaporation technique is reported suitable for preparation of CdS thin films [1-3]. Fabrication of thin films by Close spaced sublimation (CSS) technique has produced encouraging results. It offers the advantages of simple apparatus, high transport efficiency and low vacuum conditions at variable temperature ranges [4]. Moreover, fabrication of thin films by CSS at suitable parameters gives us results with favorable features such as larger grain size, well defined preferential orientation and relatively high absorption coefficient required in the solar cell applications.

In this chapter, fabrication history of different samples of CdS thin films prepared by CSS is given. This chapter deals with brief description and analysis of the physical properties of CdS thin films and silver-doped CdS thin films studied for this research.

4.1 Experimental Procedure

CdS thin films were deposited onto glass substrates by CSS technique. The substrates of size about *25* mm x *75* mm were cleaned for *30* min in pure IPA bath, by ultrasonic cleaner. CdS powder (*99.99*% pure) of Aldrich (USA) chemical company was used as source material each time for fabrication of thin film. CdS powder was put in the graphite boat of size about *20* mm x *70* mm, heated by a halogen lamp (*1000* W) connected to the main power through temperature controller with K-type thermocouple. The substrate was fixed above at a distance of 5mm from the source material. It was heated by another halogen lamp (*500* W), while the thermocouple was placed over the substrate to measure its surface temperature. Source and substrate temperatures were kept at *550* °C and *400* °C, with temperature controllers, respectively. The vacuum was created in the chamber up to $\sim 10^{-5}$ mbar with the help of rotary pump and oil diffusion

pump. The deposition time for different samples was different to attain films of variable thickness, given as in Table 4.1:

Table 4.1 Variation of thickness Vs deposition time.

Sample Name	**Deposition Time (min)**	**Thickness* (nm)**
CdS402	5	248
CdS401	6	270
CdS407	7	366
CdS410	8	369
CdS409	10	444
CdS405	15	776
CdS404	18	860

*Thickness was found by Spectrophotometer (page 82)

In the apparatus, shutter arrangement and thickness measure-meter were not available to control the thickness of thin films accurately. Because of these limitations, proper sets of samples regarding thickness variation couldn't be fabricated.

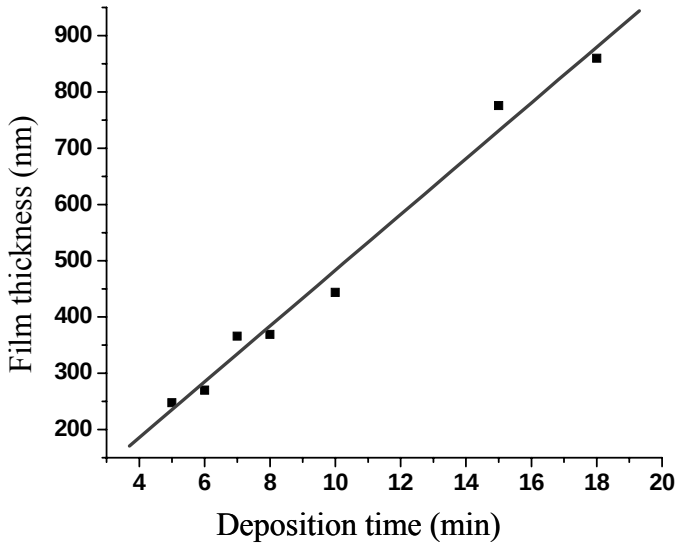

Fig 4.1 Variation of thickness as a function of deposition time.

After that the source and substrate lamps were switched off for cooling down to room temperature before opening the chamber. These thin films were then annealed at *450* °C for 30min under vacuum. All the samples were characterized by different tools for different studies. In the next step, these thin films were treated chemically by immersing in low concentrated (*0.1*g/*100* mL) $AgNo_3$-H_2o solution at room temperature for different periods of time as shown in Table 4.2:

Table 4.2 Selected immersion time (doping) with film thickness.

Sample Name	**Immersion Time (min)**	**Thickness (nm)**
CdS402	1	248
CdS401	5	270
CdS407	10	366
CdS410	15	369

CdS409	20	444
CdS405	25	776
CdS404	30	860

Thin films were cleaned in distilled water and then dried after immersion. All the samples were annealed at *450* ^{o}C under vacuum for *30* min, for diffusion of Ag into thin films. All the Ag-doped samples were characterized for the study of doping effects. The structure of the samples was studied by XRD using Cu- Kα (*1.5418* Å) radiation with operating conditions voltage/current *40* kV. The microstructure of the samples was examined using scanning electron microscopy (SEM). The SEM accelerating voltage was *10* kV. The compositions of Cd, S and Ag of all the samples were measured with the help of EDX attached to the SEM. Surface morphology of couple of the samples were further studied with the help of Atomic force microscopy (AFM). Electrical properties were measured by Ecopia Hall measurement system, at room temperature. The optical properties such as film thickness, refractive index and optical band gap were calculated from the transmission spectra between *300* nm and *2000* nm wavelength recorded by spectrophotometer. Analyses of all the characterizations are discussed here.

4.2 Structural Analysis

The structure of the as-deposited CdS and Ag-doped CdS thin films was studied using X-ray diffraction (XRD) technique. The diffraction spectra were measured at 2θ scanning mode ranging from *20* to *60* degree diffraction angle. XRD spectra of as-deposited CdS thin films are shown in Fig 4.2

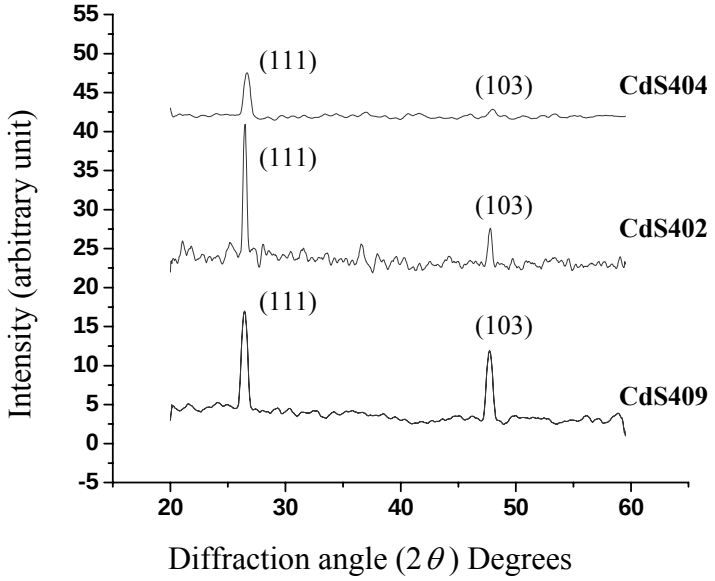

Fig 4.2 The XRD patterns of the samples 402,404,409.

Bulk CdS has either a hexagonal (wurtzite) or cubic (zinc blende) crystal structure. This structure depends on the conditions used during growth [5].

Fig. 4.2 shows the XRD spectra for the thermally evaporated thin films of different thicknesses on glass substrates. Appearance of many peaks indicates the polycrystalline nature of thin films. The major peaks in all samples appear around 2θ of *26.547*° and of *47.794*° (standard values). The XRD pattern were matched with ASTM card numbers C01-080-0019 and C00-041-1049, for peaks appeared around 2θ of *26.547*° and of *47.794*° respectively.

The main reflections are the same, in which (111) plane corresponds to the cubic system and (103) plane represents hexagonal phase in thin films growth. Intensities of reflection corresponding to (103) plane in different samples are different. However the strong reflection in all samples of thin films indicates crystallites corresponding to the (111) plane of cubic CdS (a = b = c = *5.82* Å) [6]. The lattice constant for these samples was calculated from the diffraction spectra using Bragg law and angular position of (111) diffraction peak. From the full-width at half maximum (FWHM) of the diffraction peaks,

the average crystallite size '*d*' of polycrystalline materials by applying the Scherrer formula was estimated:

$$d(\text{Å}) = k\lambda(\text{Å})/(D\cos\theta) \quad \text{.....(4.1)}$$

where the Scherrer constant k is taken equal to 0.9 [7], D is the full width at half maximum in radians and θ is the Bragg angle in degrees corresponding to the maximum peak intensity. To reduce the error in calculation of crystallite sizes and lattice parameters (a=b=c), software PC-APD version 4.0g for X-ray diffraction developed by Philips Holland was used.

Calculated crystallite sizes of samples CdS402, CdS404, CdS409 were 199nm, 160nm and 140.7nm respectively. Generally the crystallite size depends on the substrate temperature, deposition rate, film thickness and annealing temperature [8]. Calculated lattice constants of samples CdS402, CdS404, CdS409 were *5.831* Å, *5.8* Å and *5.838* Å respectively, which are very close to the reported value *5.82* Å [6]. After silver doping, XRD spectra of two samples were studied as given in Fig 4.3.

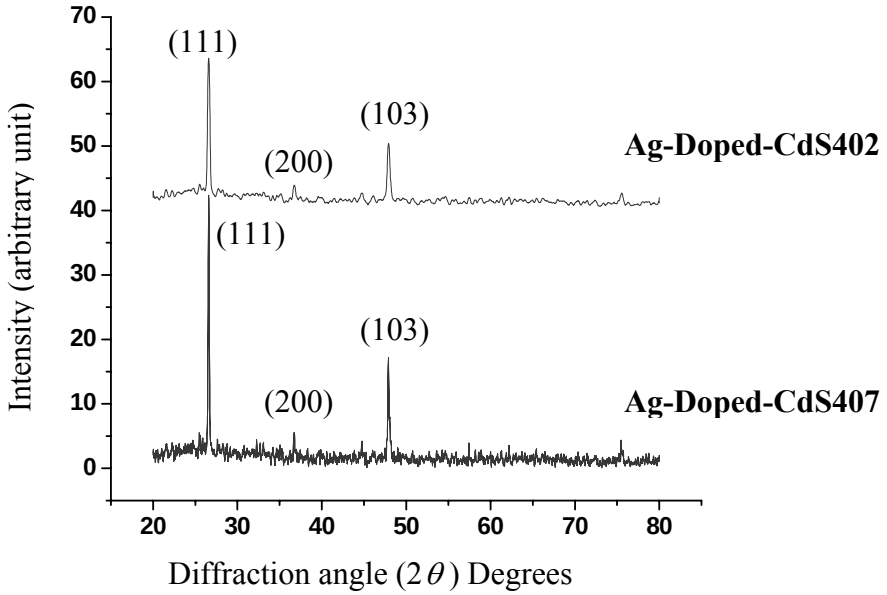

Fig 4.3 The XRD patterns of Ag-doped 402,407.

In Ag-doped CdS samples all reflections are same with as-deposited samples, except one reflection around 2θ of *36.806*° which corresponds to the (200) plane of cubic Ag_2S [9].

The peaks were matched with ASTM card number C00-004-0774. Because mass% of Ag is less as compare to the Cd and S so the intensity of peaks are small. Mass% of Ag in Sample CdS407 (*4.86*%) is larger as compare to the CdS402 (*4.36*%) so its relevant peak intensity is also greater comparatively as shown in Fig. 4.3.

4.3 Surface Study

For the surface study, scanning electron microscopy (SEM) was used. Micrographs of as-deposited CdS and Ag-doped CdS thin films are given here. Samples were scanned at different magnifications.

Here SEM micrographs are shown with order of increasing thickness of thin films.

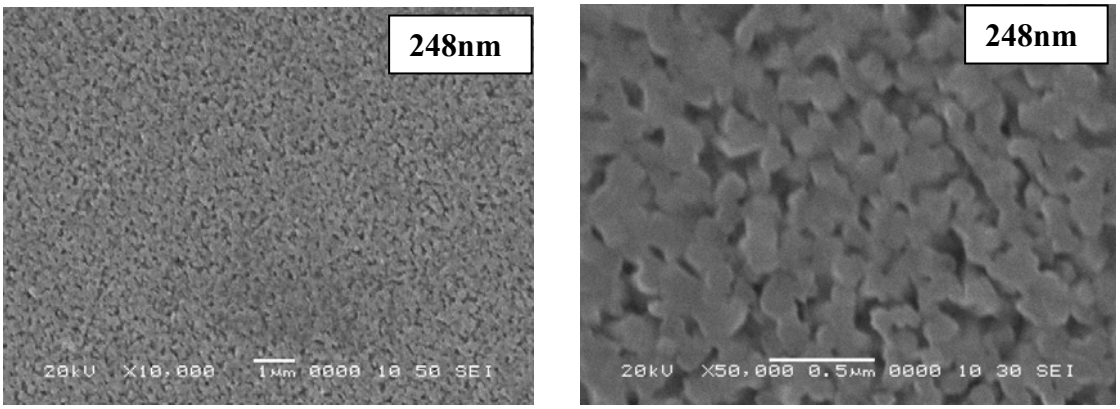

Fig 4.4 SEM graph of as-deposited CdS402.

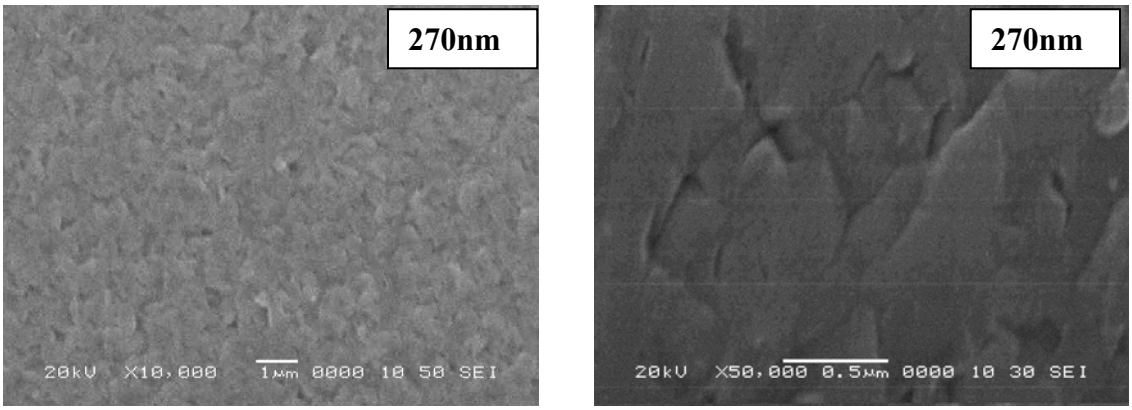

Fig 4.5 SEM graph of as-deposited CdS401.

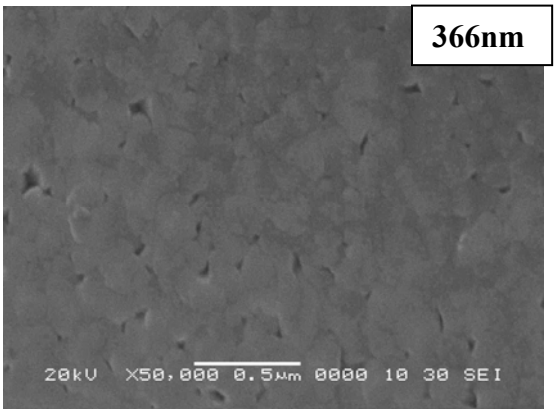

Fig 4.6 SEM graph of as-deposited CdS407.

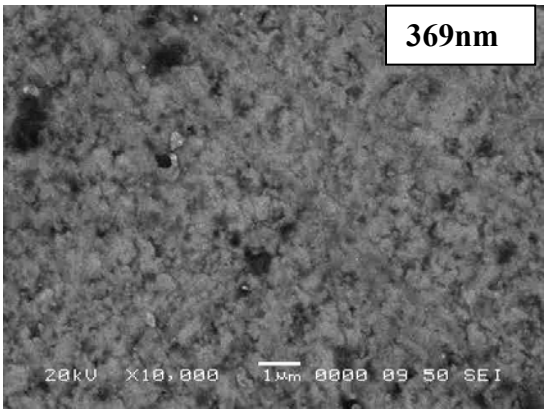

Fig 4.7 (a) SEM graph of as-deposited CdS410.

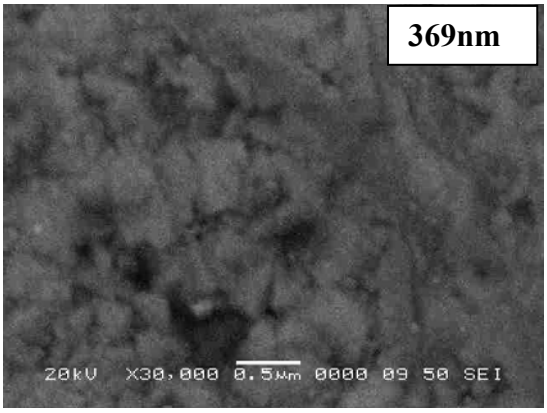

Fig 4.7 (b) SEM graph of as-deposited CdS410.

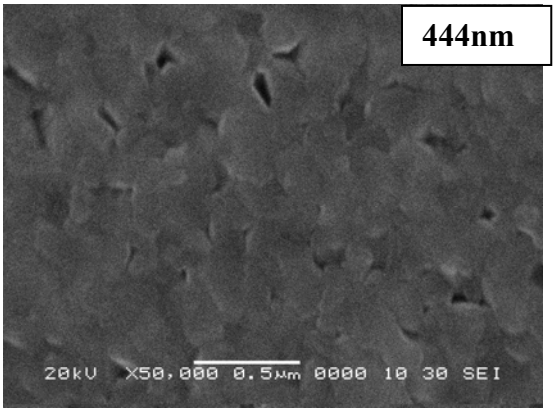

Fig 4.8 SEM graph of as-deposited CdS409.

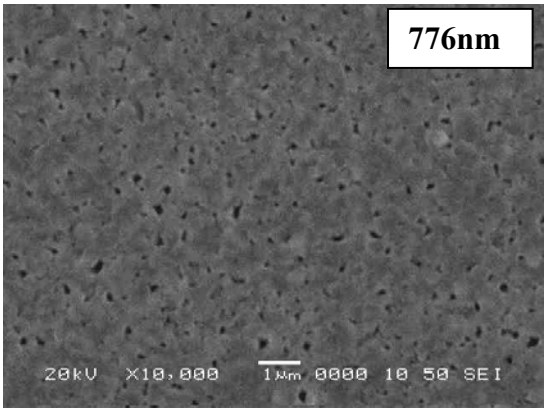

Fig 4.9 (a) SEM graph of as-deposited CdS405.

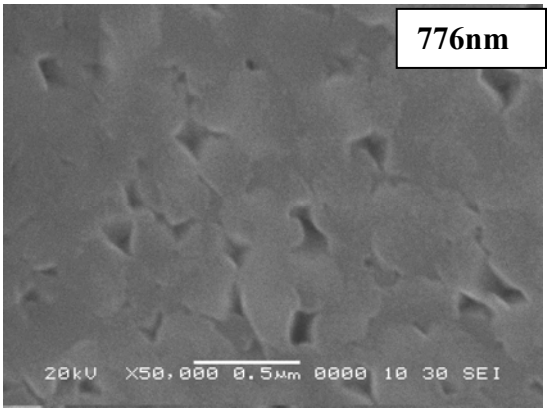

Fig 4.9 (b) SEM graph of as-deposited CdS405.

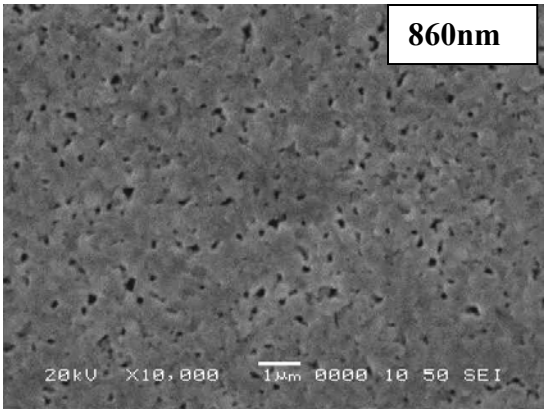

Fig 4.10 (a) SEM graph of as-deposited CdS404.

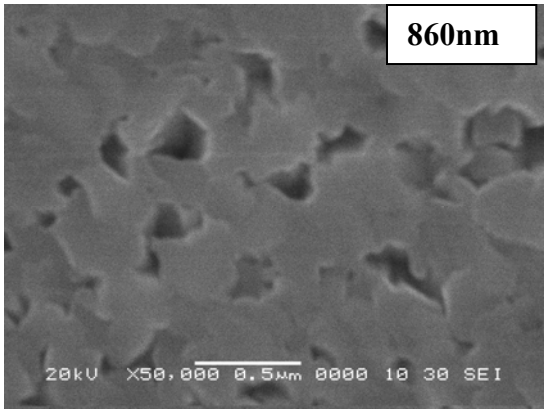

Fig 4.10 (b) SEM graph of as-deposited CdS404.

Average grain sizes of the as-deposited thin films are calculated from the SEM graphs. The values of grain sizes are different in different samples, which are given in Table 4.3. But more or less, all grains are of similar sizes in each sample. Overall in all samples, it can be seen clearly that some (closed) pores/voids are distributed. It seems that, voids in between different oriented grains were filled during annealing and this phenomenon could be supported and continued if annealing time would have increased. To confirm that the voids observed in samples are not infect pores (throughout hole), the particular area of a sample was studied by EDX analysis as shown in Fig. 4.27

Table 4.3 Variation of Grain Size and density with Film Thickness.

Sample Name	**Thickness (nm)**	**Average Grain Size (nm)**	**Dislocation density lines/m^2 (δ)**	**Grain Density (grains/m^2)**
CdS-402	248	195.7	26.1×10^{12}	15.2×10^{12}
CdS-401	270	240.3	17.3×10^{12}	7.63×10^{12}
CdS-407	366	228.3	19.1×10^{12}	14.1×10^{12}
CdS-410	369	303.4	10.8×10^{12}	8.18×10^{12}

CdS-409	444	306.9	10.6×10^{12}	7.01×10^{12}
CdS-405	776	365.4	7.4×10^{12}	4.68×10^{12}
CdS-404	860	409.5	5.9×10^{12}	3.5×10^{12}

Generally, with increasing film thickness average grain size is increased and grain density is decreased [10], as shown in Table 4.3. It shows that as thickness increases, thin film grows in better and relaxed (less defects and stresses) mode which results in larger grains. The dislocation density (δ), defined as the length of dislocation lines per unit area, has been estimated using the following equation [11]:

$$\delta = 1/D^2 \quad \text{.....(4.2)}$$

Where D is the grain size of thin film and (δ) is the measure of amounts of defects in a crystal. Small amount of defects showed good crystallinety in grown CdS thin films.

After silver doping with different mass% ratios, samples were characterized to study the surface morphology. Here SEM micrographs are given in order of increasing mass% ratio of silver content. The ratios of the Cd, S and Ag were determined by using Energy Dispersive X-ray Spectroscopy (EDX).

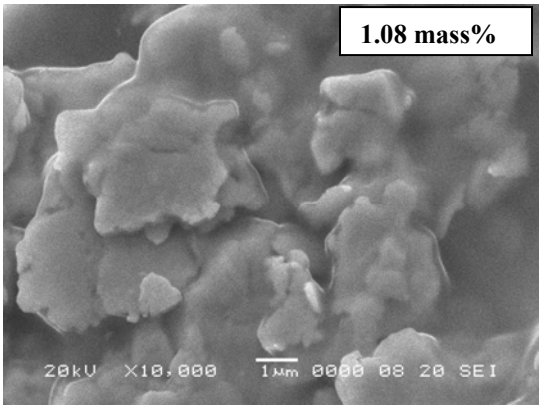

Fig 4.11 SEM graph of Ag-doped-CdS401.

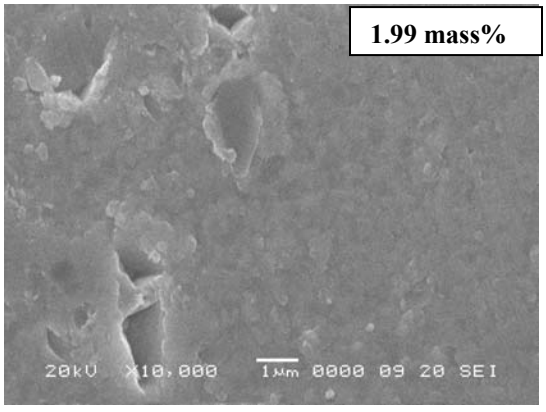

Fig 4.12 SEM graph of Ag-doped-CdS410.

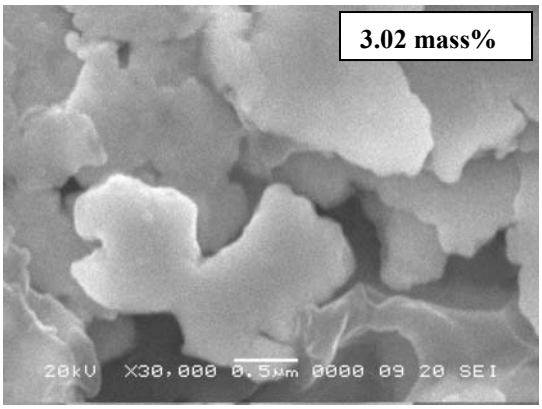

Fig 4.13 SEM graph of Ag-doped-CdS405.

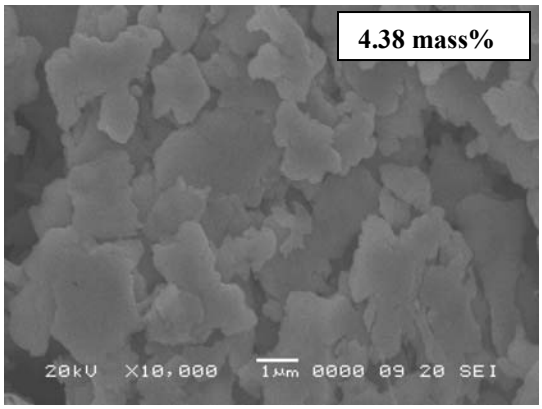

Fig 4.14 SEM graph of Ag-doped-CdS402.

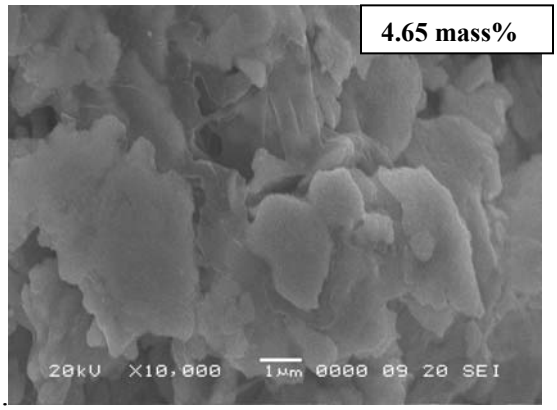

Fig 4.15 SEM graph of Ag-doped-CdS409.

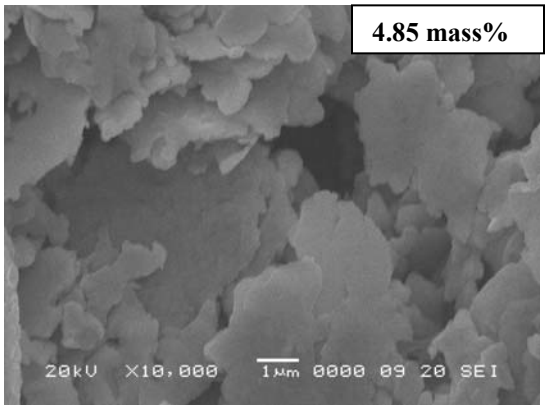

Fig 4.16 SEM graph of Ag-doped-CdS407.

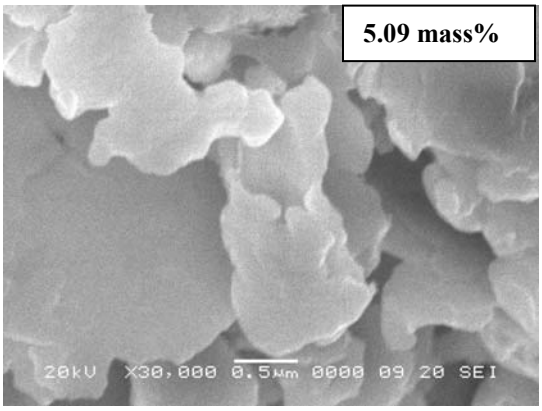

Fig 4.17 SEM graph of Ag-doped-CdS404.

In as-deposited CdS thin films, it was observed that all grains are roughly of similar sizes in almost every sample. But in Ag-doped case, from surface study it is clear that grains in each sample are distributed in different sizes.

Let us compare couple of samples before Ag-doping and after Ag-doping.

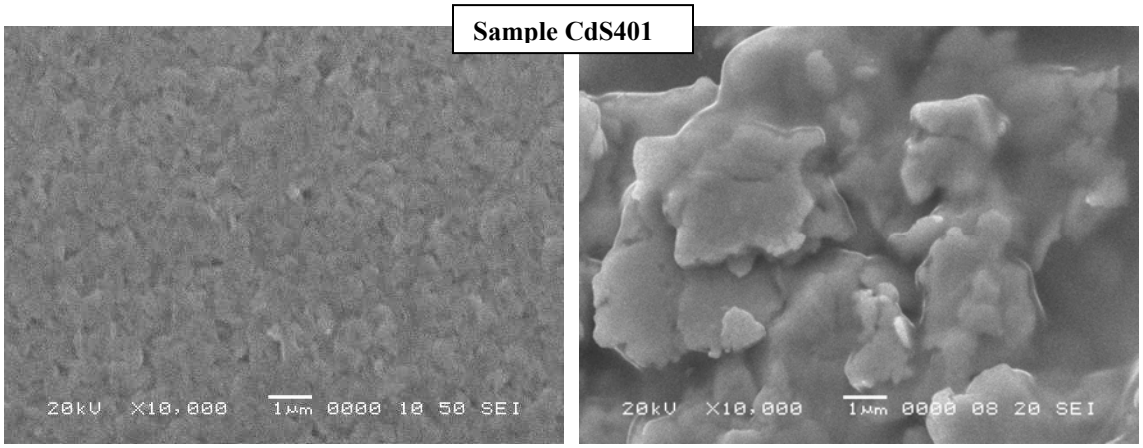

Fig 4.18(a) Before Ag-doping. **Fig 4.18(b)** After Ag-doping.

In ion exchange mechanism, atoms of the doped species can be added into the parent material at interstitial sites and/or substitutional sites depending upon the size of atoms and sites available. In this case, it can be explained with interstitial-substitution diffusion with kick-out mechanism [12]. As the silver ions start diffusing they place themselves at interstitial sites and then later on they displace some of Cd-atoms which were already placed. Then Ag-ions become self-interstitial into the CdS lattice by forming Ag_2S. The process of forming Ag_2S crystallization is supported by the annealing process.

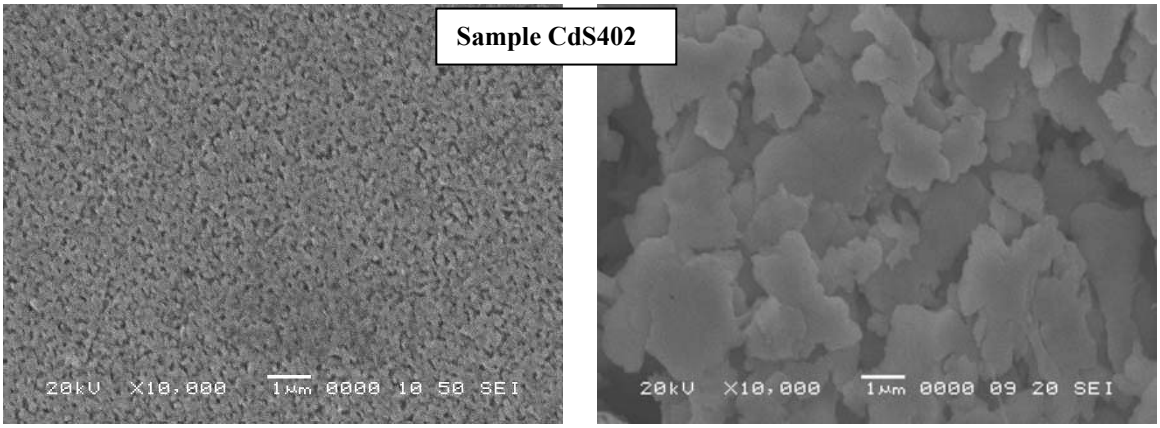

. **Fig 4.19(a)** Before Ag-doping. **Fig 4.19(b)** After Ag-doping.

From SEM micrographs of Sample CdS401 and CdS402, it can be observed that grain sizes after Ag-doping are increased drastically. After doping, surface is not looking smooth also as compared to the as-deposited samples. It seems that concentration of silver is more on surface as compared to the concentration of silver in depth of thin film. Samples were annealed for *30* min after Ag-doping, but silver atoms are not diffused well inside throughout (up to all depth) the sample because of less annealing time. Hence in this case, Ag-modified thin films can be presented more or less as CdS- Ag_2S double layer thin films. However it doesn't mean that Ag-atoms are not diffused in CdS-layer and there is no Cd-atoms present in Ag_2S-layer. But it would be better to say that there is difference in concentration of Silver atoms in both regimes (CdS- Ag_2S). It is also expected that upper layer (Ag-enriched comparatively) has very minute thickness as compare to the thickness of the whole sample [13].

Elemental (Cd, S, Ag) ratios, determined by EDX graphs are shown here. EDX graphs of before doping thin films are shown in increasing order of thickness here.

Processing option : All elements analyzed (Normalised)
Number of iterations = 2

Element	Weight%	Atomic%
S K	24.26	52.89
Cd L	75.74	47.11
Totals	100.00	

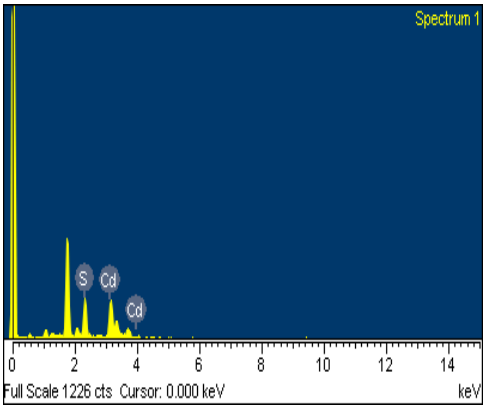

Fig 4.20 EDX of CdS-402

Processing option : All elements analyzed (Normalised)
Number of iterations = 2

Element	Weight%	Atomic%
S K	21.82	49.45
Cd L	78.18	50.55
Totals	100.00	

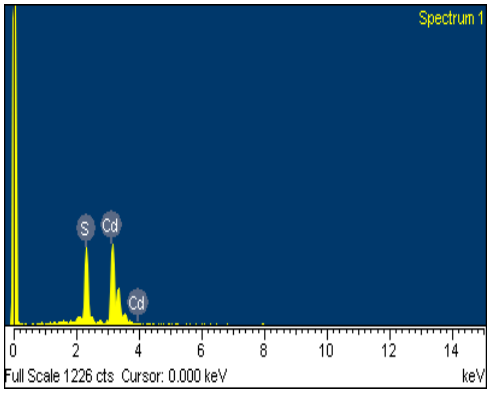

Fig 4.21 EDX of CdS-401.

Processing option : All elements analyzed (Normalised)
Number of iterations = 2

Element	Weight%	Atomic%
S K	23.55	51.92
Cd L	76.45	48.08
Totals	100.00	

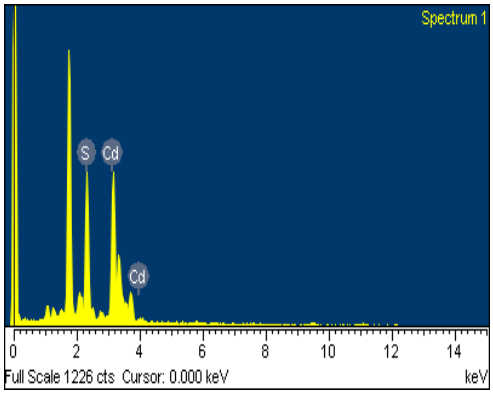

Fig 4.22 EDX of CdS-407

Processing option : All elements analyzed (Normalised)
Number of iterations = 2

Element	Weight%	Atomic%
S K	23.00	51.15
Cd L	77.00	48.85
Totals	100.00	

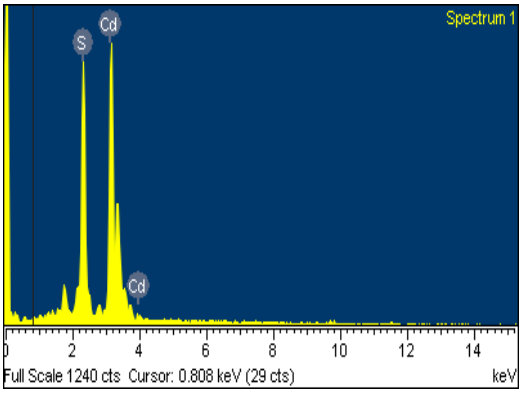

Fig 4.23 EDX of CdS-410.

Processing option : All elements analyzed (Normalised)
Number of iterations = 2

Element	Weight%	Atomic%
S K	21.13	48.44
Cd L	78.87	51.56
Totals	100.00	

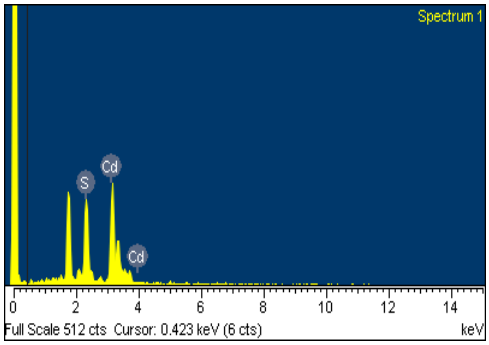

Fig 4.24 EDX of CdS-409.

Processing option : All elements analyzed (Normalised)
Number of iterations = 2

Element	Weight%	Atomic%
S K	22.49	50.42
Cd L	77.51	49.58
Totals	100.00	

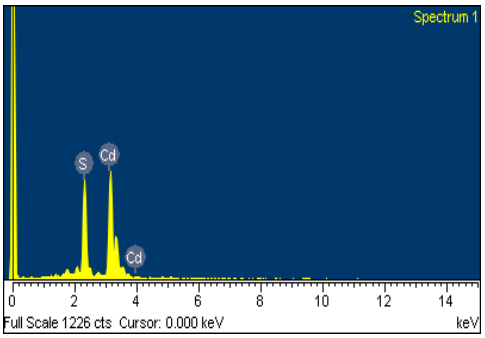

Fig 4.25 EDX of CdS-405.

Processing option : All elements analyzed (Normalised)
Number of iterations = 3

Element	Weight%	Atomic%
S K	22.96	51.09
Cd L	77.04	48.91

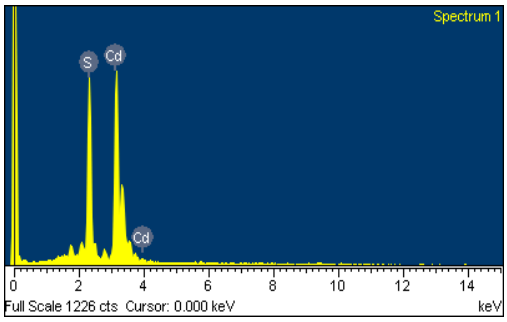

Fig 4.26 EDX of CdS-404.

When CdS is sublimated, at higher temperature CdS compound dissociates into the Cd and S. At substrate or near substrate, it again makes chemical bond and takes form into CdS compound. So that depending upon different factors, ratio of Cd and S is different in different samples. Atomic weight of CdS compound is *144.4* (112.4+32.066), so its starting composition (CdS powder) is:

Cd = 112.4/144.466 = 0.778 = 77.8%

S = 32.066/ 144.46 = 0.222 = 22.2%

Its end composition (after deposition), according to the EDX data is shown in Table 4.4

Table 4.4 End composition of CdS after deposition.

Sample	Composition (Cd/S)	$Cd_{(1\pm x)}S_{(1\pm x)}$
401	78.18/21.82	$Cd_{(1.01)}S_{(0.99)}$
402	75.74/24.25	$Cd_{(0.98)}S_{(1.02)}$
404	77.04/22.96	$Cd_{(0.99)}S_{(1.01)}$
405	77.51/22.49	$Cd_{(0.99)}S_{(1.01)}$
407	76.45/23.55	$Cd_{(0.99)}S_{(1.01)}$
409	78.87/21.13	$Cd_{(1.01)}S_{(0.99)}$
410	77.00/23.00	$Cd_{(0.99)}S_{(1.01)}$

From Table 4.4, it is clear that end composition changed slightly from the starting composition.

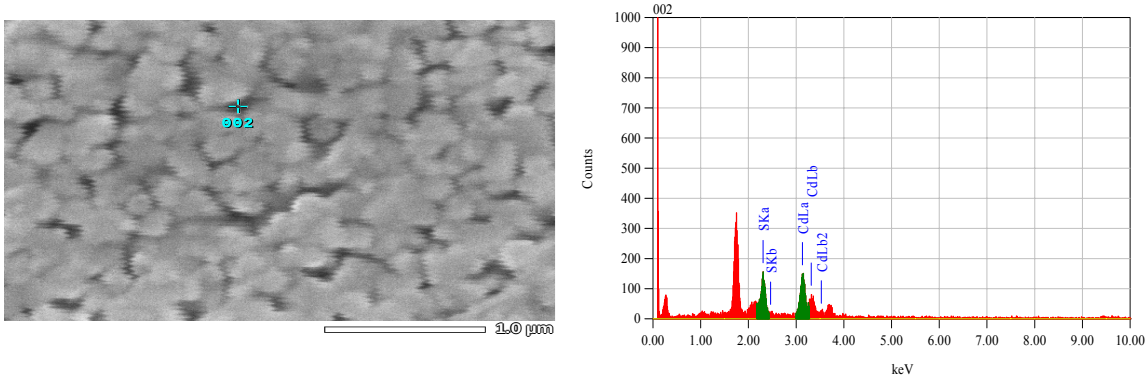

Element	(keV)	Mass%	Error%	Atom%
S K*	2.307	21.43	2.08	48.88
Cd L*	3.132	78.57	7.63	51.12
Total		100.00		100.00

Fig 4.27 point probe EDX of CdS-402.

From EDX analysis of particular region (voids), we confirmed that these are not pores but in fact these are voids. In EDX data of the particular region, the mass% ratio was approaching the mass% obtained in whole area scan.

After doping of Silver (Ag) by ion exchange process, these samples were characterized to determine the Ag ratio in the different samples. EDX graphs of Ag-doped samples are given here. EDX graphs are given in order of increasing Ag-ratio in different samples.

Processing option : All elements analyzed (Normalised)
Number of iterations = 2

Element	Weight%	Atomic%
S K	22.75	50.78
Ag L	**1.08**	**0.72**
Cd L	76.17	48.50
Totals	100.00	

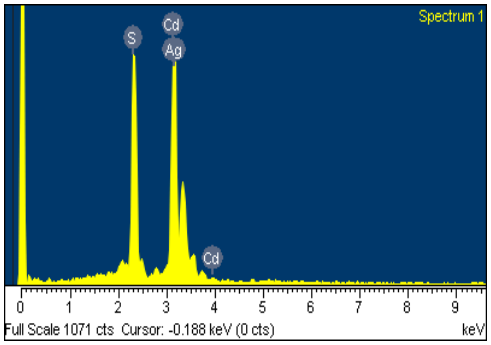

Fig 4.28 EDX of doped CdS-401.

Processing option : All elements analyzed (Normalised)
Number of iterations = 3

Element	Weight%	Atomic%
S K	22.88	50.95
Ag L	**1.99**	**1.32**
Cd L	75.13	47.73
Totals	100.00	

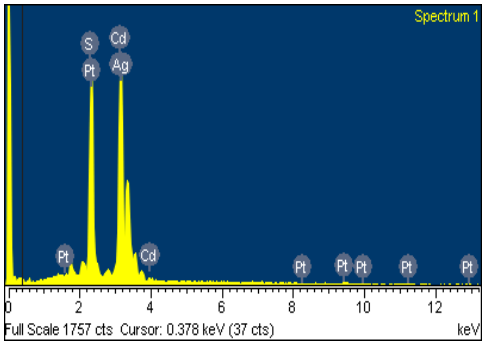

Fig 4.29 EDX of doped CdS-410.

Processing option : All elements analyzed (Normalised)
Number of iterations = 3

Element	Weight%	Atomic%
S K	21.96	49.62
Ag L	**3.02**	**2.03**
Cd L	75.02	48.36
Totals	100.00	

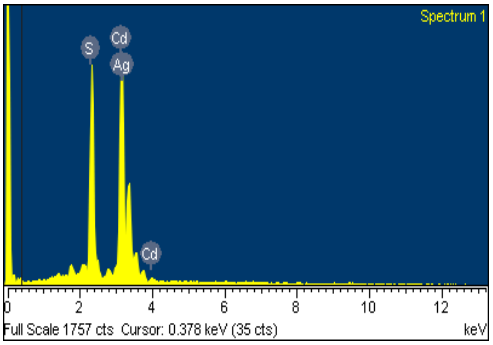

Fig 4.30 EDX of doped CdS-405.

Processing option : All elements analyzed (Normalised)
Number of iterations = 2

Element	Weight%	Atomic%
S K	21.92	49.54
Ag L	**4.38**	**2.94**
Cd L	73.70	47.52
Totals	100.00	

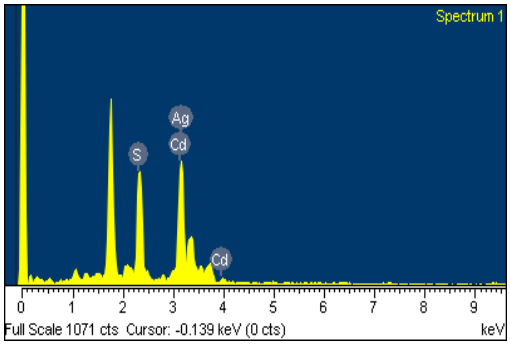

Fig 4.31 EDX of doped CdS-402.

Processing option : All elements analyzed (Normalised)
Number of iterations = 2

Element	Weight%	Atomic%
S K	22.15	49.88
Ag L	**4.65**	**3.11**
Cd L	73.20	47.01
Totals	100.00	

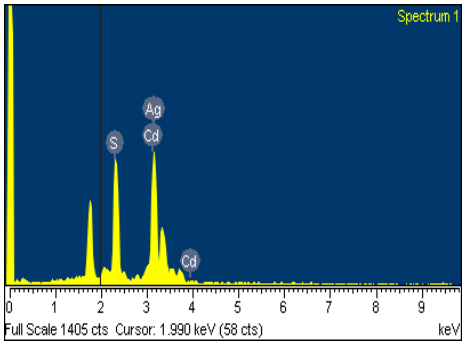

Fig 4.32 EDX of doped CdS-409.

Processing option : All elements analyzed (Normalised)
Number of iterations = 2

Element	Weight%	Atomic%
S K	22.66	50.60
Ag L	**4.86**	**3.23**
Cd L	72.48	46.17
Totals	100.00	

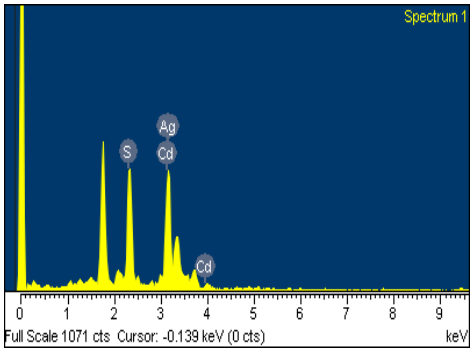

Fig 4.33 EDX of doped CdS-407.

Processing option : All elements analyzed (Normalised)
Number of iterations = 3

Element	Weight%	Atomic%
S K	22.55	50.44
Ag L	**5.09**	**3.38**
Cd L	72.36	46.17

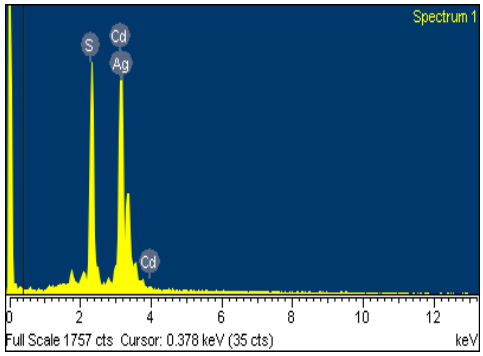

Fig 4.34 EDX of doped CdS-404.

Different samples were immersed in $AgNo_3$-distilled water solution (*0.1* g/*100* ml) for different times, given in Table 4.5;

Table 4.5 Immersion Time and Ag-ratio in CdS thin films.

Sample	Thickness (nm)	Immersion Time(min)	Ag Weight%
CdS-401	270	5	1.08
CdS-410	369	15	1.99
CdS-405	776	25	3.02
CdS-402	248	1	4.38
CdS-409	444	20	4.65
CdS-407	366	10	4.86
CdS-404	860	30	5.09

By definition, Ag-ratio in CdS thin film should have increased with increasing immersion time. In this case, due to different sets of film thickness Ag-ratio were obtained also different.

4.3.1 Topographical Study

For further study of surface, topographical images of three samples were taken through atomic force microscopy (AFM). Tapping mode AFM was employed for surface characterization. All of the scanning was carried out at room temperature.

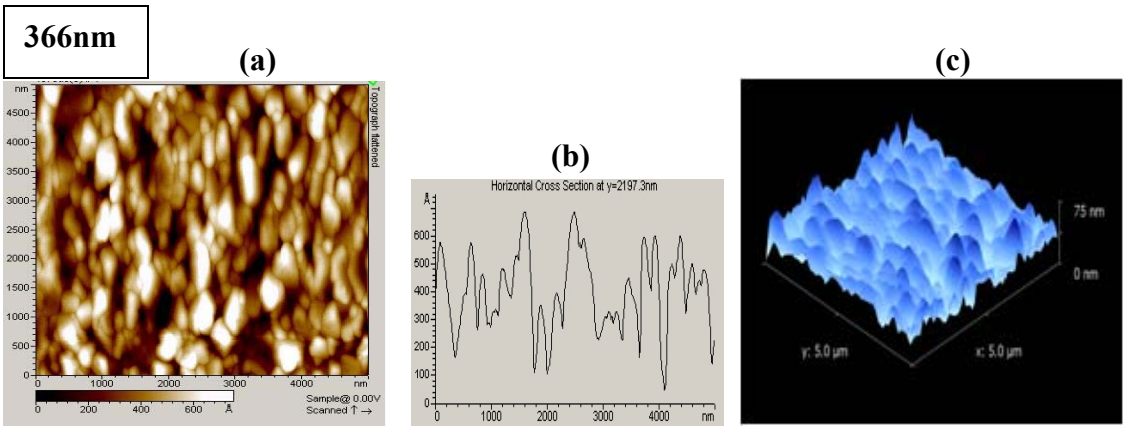

Fig. 4.35 AFM images of CdS407 (a) 2D image, (b) line profile of 2D and (c) 3D image.

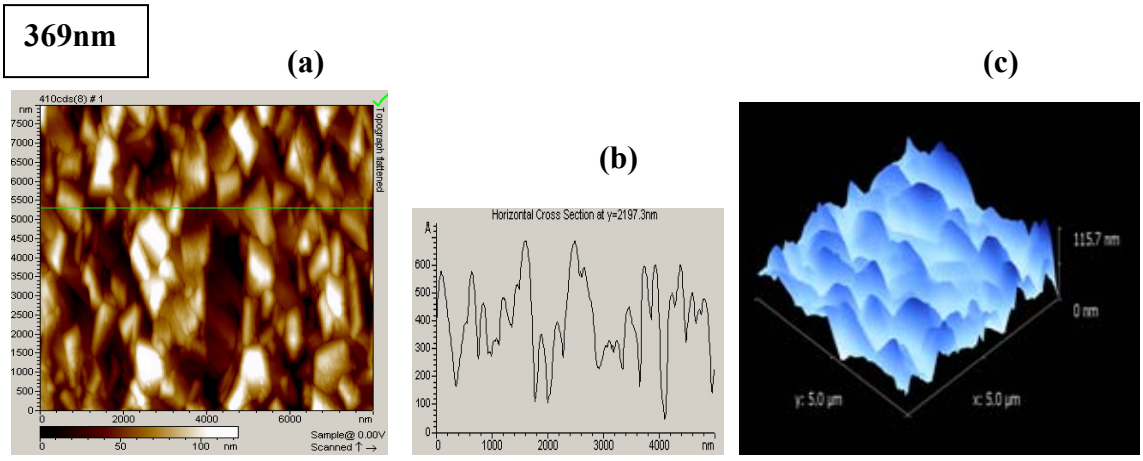

Fig. 4.36 AFM images of CdS410 (a) 2D image, (b) line profile of 2D and (c) 3D image.

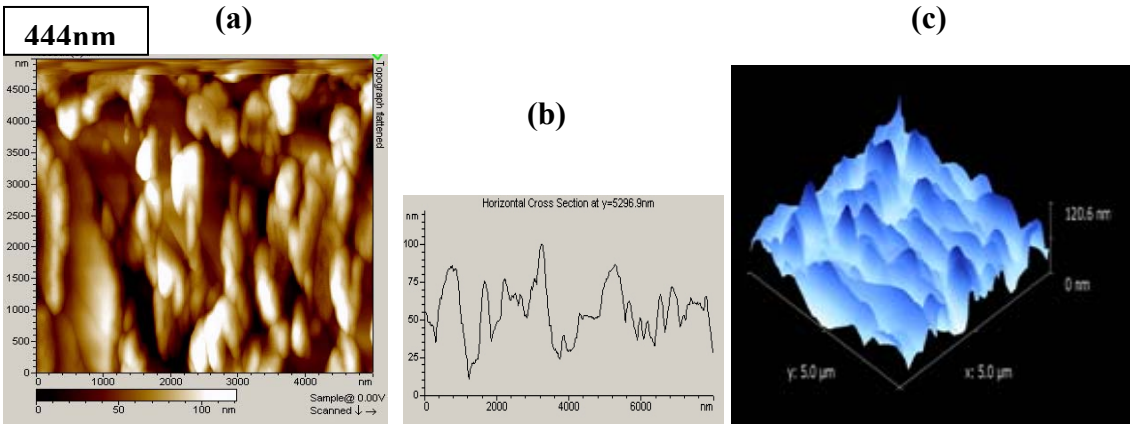

Fig. 4.37 AFM images of CdS409 (a) 2D image, (b) line profile of 2D and (c) 3D image.

From AFM images, the average grain sizes and grain densities of samples were confirmed. The values of average grain sizes and grain densities calculated from AFM

images were approaching to the values calculated from SEM images. From surface profile average surface roughness is obtained given in Table 4.6:

Table 4.6 Surface Roughness as function of Thickness.

Sample name	Thickness(nm)	Surface Roughness(nm)
CdS407	366	15.52
CdS410	369	44.7
CdS409	444	99.40

From AFM studies, it was observed that our samples showed behavior of increasing surface roughness with increase in thickness, which is a good agreement with reported results in literature [14-16].

4.4 Optical Analysis

The study of optical properties, as transmission, refractive index and energy gap are of great importance regarding any material used in opto-electronic applications. The UV-VIS/NIR spectrophotometer (Perkin Elmer Lambda 950) and UV-WinLab software were used to measure the transmission spectra of all samples (before and after doping). All other (mentioned) parameters were calculated from transmission spectra. The transmission spectra of as-deposited samples are shown in figure 4.38.

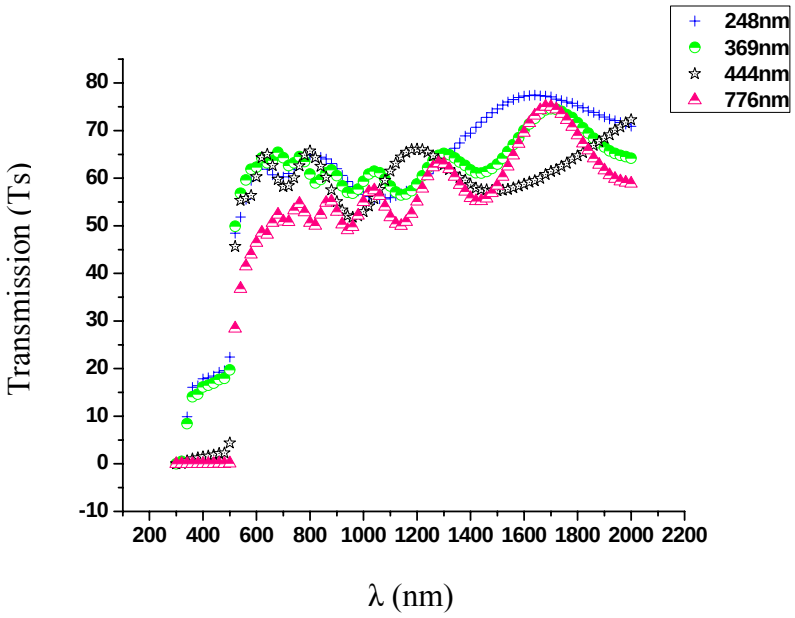

Fig. 4.38 Transmission (Ts) curves of un-doped samples

Transmission spectra of as-deposited CdS thin films of various thickness show the light transmission from *50*% to *80*% in the visible region [17]. As the thickness of samples was increased, there was decrease in the transmission as shown in Fig 4.38. A sudden fall in transmission about the wavelength of *500* nm (~2.42 eV) shows that, band gap of CdS occurs in this region. The ultraviolet rays and x-rays are absorbed as these have more energy than the energy band gap of cadmium sulfide. On the other hand the entire wavelength of visible and near infrared region is transmitted. So the cadmium sulfide is a window material for the visible region as well as for infrared region.

From Swanepoel model, the refractive index and thickness of the thin films can be calculated [18].

The refractive index (n) can be calculated as

$$n = \frac{[N + (N^2 - 4s^2)^{\frac{1}{2}}]}{2} \quad \ldots\ldots\ldots\ldots\ldots\ldots\ldots\ldots\ldots\ldots\ldots\ldots\ldots\ldots (4.3)$$

Where '*s*' is refractive index of the substrate (1.25), N is number of oscillations

$$N = 1 + s^2 + 4s(\frac{T_M - T_m}{T_M T_m}) \ldots\ldots\ldots\ldots\ldots\ldots\ldots\ldots\ldots\ldots\ldots\ldots\ldots\ldots (44.)$$

Where T_M and T_m are the Transmission maxima and minima, respectively. Thickness of the films can be calculated with the help of formula

$$d = \frac{1}{4n}[\frac{\lambda_m \lambda_M}{\lambda_M - \lambda_m}], \ldots\ldots\ldots\ldots\ldots\ldots\ldots\ldots\ldots\ldots\ldots\ldots\ldots\ldots\ldots\ldots (4.5)$$

Where 'd' is the thickness λ_m is the minima and λ_M is the maximum value of the wavelength taken from the transmission curves.

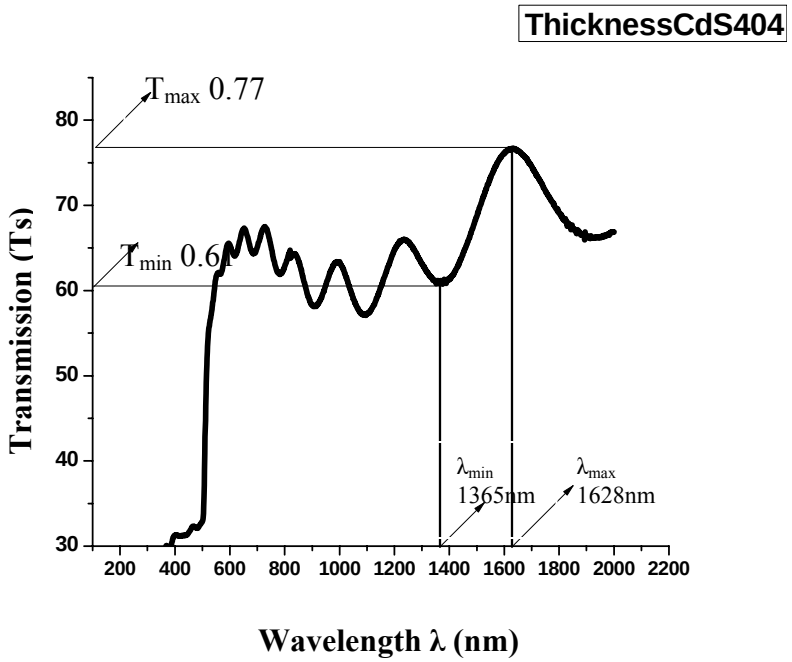

Fig. 4.39 Transmission (Ts) curve of un-deposited CdS404.

By using same method, refractive index and thickness of thin films were calculated for all as-deposited thin films samples as given in Table 4.7;

Table 4.7 Values of Calculated Refractive Index and Thickness.

Sample	**λ_{max} (nm)**	**λ_{min} (nm)**	**T_{max}**	**T_{min}**	**N**	***n***	**Thickness (nm)**
401CdS	1700	1000	0.65	0.55	4.93	2.25	270
402CdS	1620	1065.57	0.78	0.55	6.47	3.14	248
404CdS	1628.12	1365.97	0.77	0.61	5.29	2.47	860
405CdS	1689.69	1427.54	0.75	0.55	6.16	2.97	776
407CdS	1689.69	1112.22	0.79	0.65	4.89	2.23	366
409CdS	1197.11	958.29	0.66	0.52	5.69	2.69	444
410CdS	1697.16	1081.43	0.73	0.63	4.56	2.02	369

Values of refractive index (*n*) vary from *2.02* to *3.13* in different samples and thickness calculated varies from *248* nm to *860* nm, as shown in Table. 4.7. Value of refractive index depends upon wavelength of light passing through medium. Behavior of refractive index with increase in wavelength was studied by spectrophotometer. Value of refractive index was decreasing with increase in wavelength (nm). Behavior of as-deposited CdS401 thin film regarding refractive index as a function of wavelength is shown in Fig.4.40.

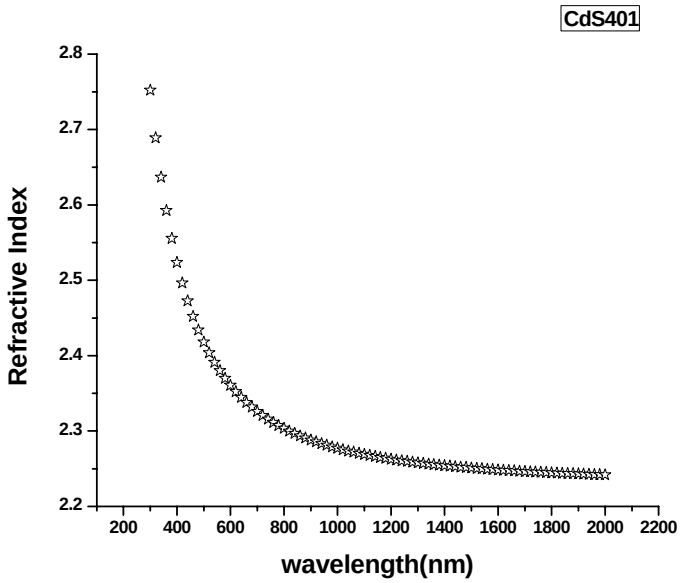

Fig. 4.40 Refractive Index Vs Wavelength (*nm*).

To confirm values of thickness calculated with the help of spectrophotometer, sample CdS402 was examined by SEM image (edge view) as shown below.

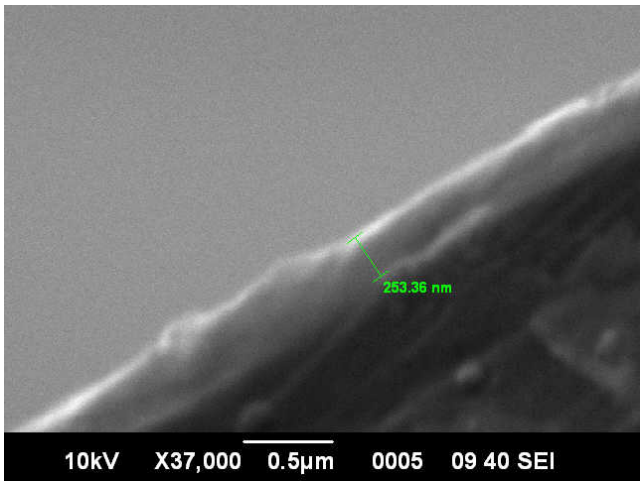

Fig. 4.41 SEM image (edge view) of CdS402.

Value of thickness calculated from SEM micrograph confirmed the accuracy of values measured by spectrophotometer.

Energy band gap was calculated by finding out the particular point (wavelength), where transmission increased abruptly, in transmission spectra of thin films (see Fig. 4.42). By using the equation;

$$E_g = \frac{hc}{\lambda} \quad \text{.....(4.6)}$$

We can calculate the value of band gap.

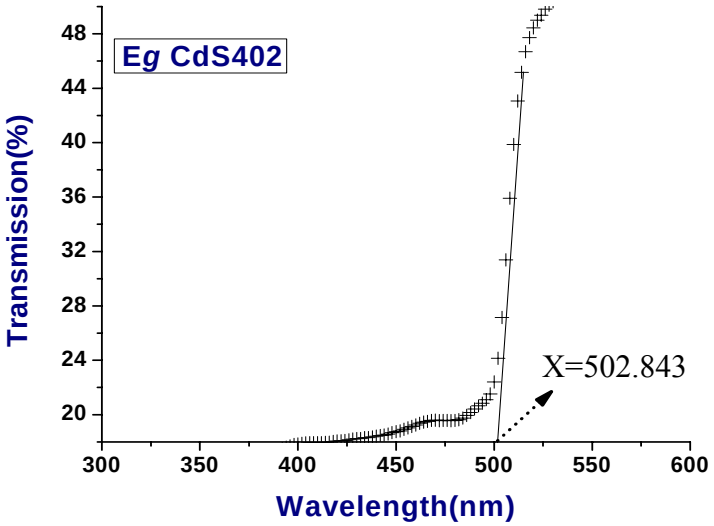

Fig.4.42 Calculation of energy band gap of CdS402

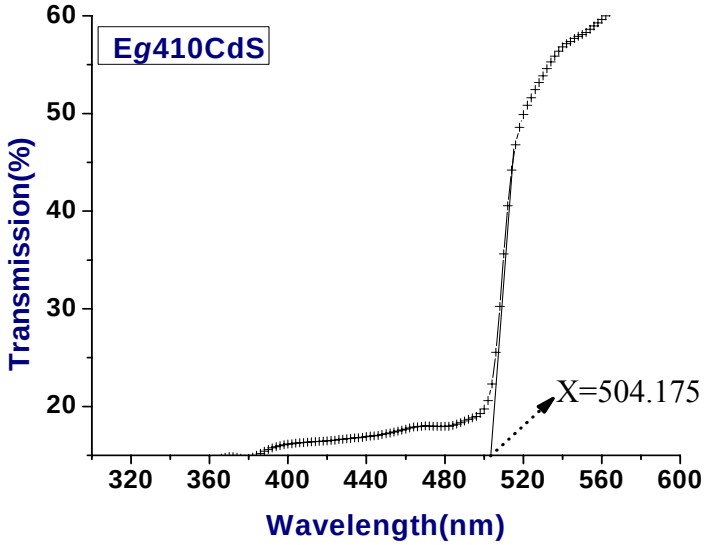

Fig.4.43 Calculation of energy band gap of CdS410.

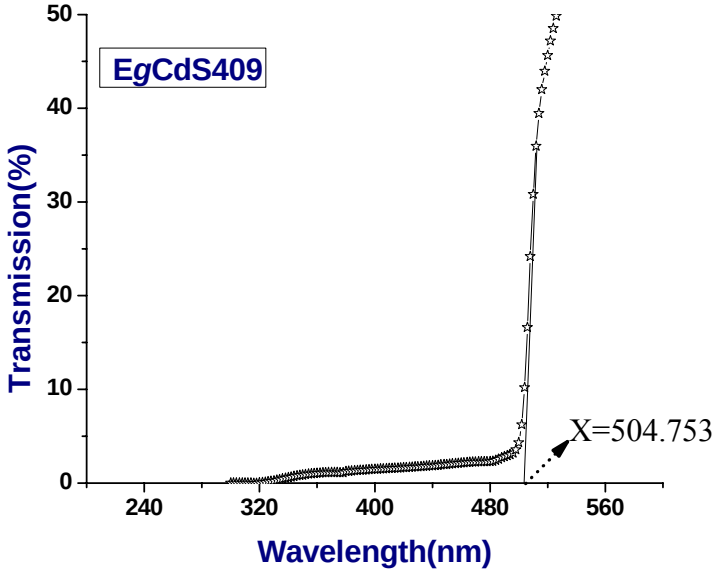

Fig.4.44 Calculation of energy band gap of CdS409.

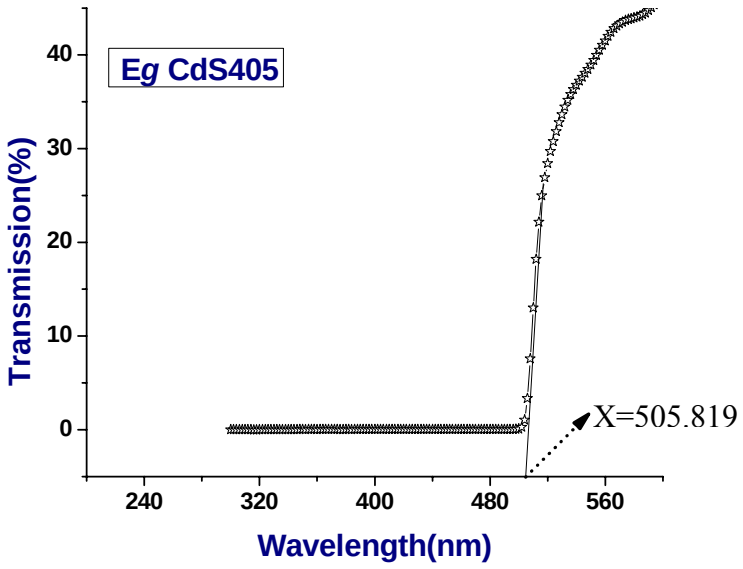

Fig.4.45 Calculation of energy band gap of CdS405.

By putting the values of *h,c* and corresponding wavelength in the above equation, we can find out the band gap of samples. Calculated values of band gaps are given in Table.4.8.

Table.4.8 Values of Energy band gaps (ev) Vs Thickness (nm).

sample	**Thickness (*nm*)**	**Wavelength (*nm*)**	**Band gap (*ev*)**
CdS402	248	502.843	2.471
CdS410	369	504.175	2.465
CdS409	444	504.753	2.462
CdS405	776	505.819	2.457

It is observed that with increase in film thickness, values of band gap slightly decreased [19].

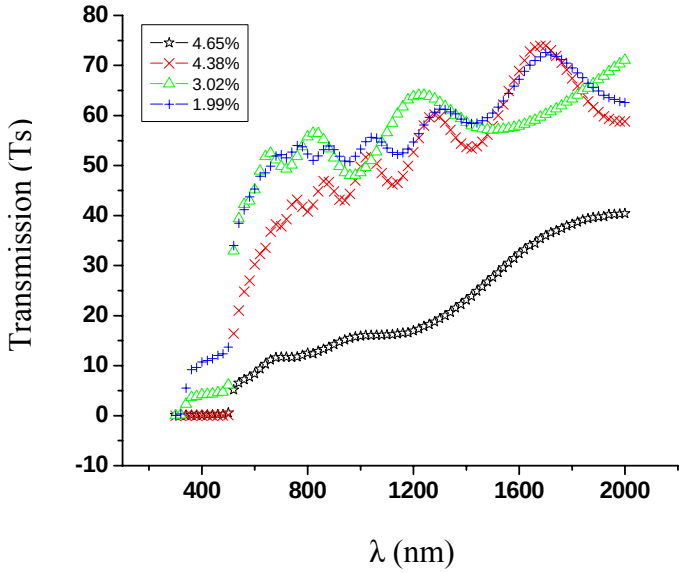

Fig. 4. 46 Transmission (Ts) curves of Ag-doped samples

From transmission spectra of Ag-doped samples, it is clear that transmission has decreased from *50-80*% (un-doped) to *40-70*% because silver is a good reflector material. With increase in silver mass% in samples, transmission is gradually decreased.

Table. 4.9 Values of Calculated Refractive Index before and after doping.

Sample	***n (before doping)***	***n* (after doping)**
401CdS	2.25	2.27
404CdS	2.47	2.45
405CdS	2.96	3.14
407CdS	2.22	3.92
409CdS	2.69	3.08
410CdS	2.02	2.34

From comparison of values of refractive index before and after doping, it is cleared that values of refractive index are increased after doping of silver in samples.

Values of energy band gap are also calculated after silver doping in samples as given in Table 4.10.

Table. 4.10 Values of Energy band gap Vs Ag-mass%.

Sample	**Ag (mass%)**	**E*g (ev)***
410CdS	1.99	2.458
405CdS	3.02	2.449
409CdS	4.38	2.444
402CdS	4.65	2.443

From given data, it is concluded that there is no significant change appeared in band gap after doping of silver [20]. However band gap could be changed with doping of larger silver (mass%) content.

4.5 Electrical Properties

Electrical properties such as resistivity, mobility and sheet concentration were measured by the Hall Measurement system (Ecopia HMS 3000). The electrical properties of un-doped CdS samples were measured at temperature of 300 K. These properties are discussed one by one here.

Resistivity of different samples and its variation with thickness is given in Table 4.11.

Table 4.11 Variation of Resistivity Vs Thickness.

Sample	**Thickness (nm)**	**Resistivity (ohm-cm)**
CdS402	248	*5.325E+7*
CdS401	270	*1.122E+6*
CdS407	366	*2.685E+8*
CdS410	369	*1.228E+5*
CdS409	444	*1.103E+5*
CdS405	776	*9.744E+4*
CdS404	860	*8.474E+3*

From given table, it is cleared that overall value of resistivity decreased with increasing thickness of our samples. The change in resistivity can be related to the change in grain size of sample [21-22]. As grain size is being increased, defects are going to be decreased so that resistivity is also decreased. Its value ranges from *2.685E+8* ohm-cm *to 8.474E+3* ohm-cm.

Mobility of different samples and its variation with thickness is given in Table 4.12.

Table 4.12 Variation of Mobility Vs Thickness.

Sample	**Thickness (nm)**	**Mobility (cm^2/Vs)**
CdS402	248	*1.524E+1*
CdS401	270	*4.97E+1*
CdS407	366	*1.050E+2*
CdS410	369	*3.783E+2*
CdS409	444	*5.603E+2*
CdS405	776	*2.227E+2*
CdS404	860	*6.110E+2*

Mobility is being increased with increase in thickness of samples. As mobility directly depends upon conductivity and conductivity is inversely proportional to the resistivity so reason is obvious for increase in mobility as narrated for resistivity.

After doping of silver, change in mobility and resistivity of samples are discussed here. Variation in resistivity before and after doping is discussed in Table 4.13.

Table 4.13 Variation of Mobility Before and After doping.

Sample	Thickness (nm)	Mobility (cm^2/Vs) un-doped	Mobility (cm^2/Vs)Ag-doped
CdS402	248	*1.524E+1*	*1.260E+4*
CdS401	270	*4.97E+1*	*1.521E+4*
CdS407	366	*1.050E+2*	*2.215E+4*
CdS410	369	*3.783E+2*	*1.481E+4*
CdS409	444	*5.603E+2*	*5.265E+3*
CdS405	776	*2.227E+2*	*3.250E+3*
CdS404	860	*6.110E+2*	*8.452E+3*

Mobility of samples is increased after doping of silver in CdS thin films. Value of mobility increased from *1.524E+1* (cm^2/Vs) *to 1.260E+4* (cm^2/Vs). Variation in conductivity before and after doping is discussed in Table 4.14.

Table 4.14 Variation of Resistivity before and after doping.

Sample	Thickness (nm)	Resistivity (ohm-cm) un-doped	Resistivity (ohm-cm)Ag-doped
CdS402	248	*5.325E+7*	*2.203E+4*
CdS401	270	*1.122E+6*	*2.047E+4*
CdS407	366	*2.685E+8*	*2.420E+4*
CdS410	369	*1.228E+5*	*7.125E+3*
CdS409	444	*1.103E+5*	*2.735E+3*
CdS405	776	*9.744E+4*	*2.751E+3*
CdS404	860	*8.474E+3*	*2.180E+3*

Values of Resistivity decreased from *2.685E+8* ohm-cm *to 2.180E+3* ohm-cm by doping of silver in CdS thin films. The value of resistivity could be decreased to more lower values by increasing mass% of silver ratio in CdS thin films.

Behavior of resistivity as a function of current for undoped and Ag-doped samples is shown in Table 4.15.

Table.4.15 Behavior of Resistivity Vs Current (a) as-deposited sample (b) Ag-doped sample.

Current (nA)	Resistivity (ohm-cm) undoped	Resistivity (ohm-cm) Ag-doped
1	*7.827E+4*	*2.198E+10*
3	*3.065E+9*	*2.818E+10*
5	*1.736E+3*	*1.827E+11*
7	*1.122E+6*	*2.288E+11*
9	*1.081E+5*	*4.519E+11*
11	*1.401E+7*	*5.212E+11*

13	*7.145E+4*	*5.536E+11*
15	*1.439E+4*	*5.862E+11*
17	*1.185E+4*	*3.078E+11*
19	*4.982E+3*	*6.082E+11*
21	*9.278E+3*	*7.842E+11*
23	*7.195E+3*	*9.982E+11*
25	*6.763E+3*	*1.615E+12*
28	*9.056E+3*	*9.039E+12*
31	*7..101E+3*	*1.334E+12*
34	*8.289E+3*	*9.892E+12*
37	*8.956E+3*	*3.638E+13*
40	*7.994E+3*	*1.797E+12*
43	*7.510E+3*	*2.445E+12*

In un-doped sample, behavior of resistivity is decreasing with increasing in current because of force applied (push) to mobile faster the charge carriers in material. However in case of Ag-doped case, increasing behavior of resistivity with current might be due to rush of charge carriers. As we apply current, more charge carriers get into free and take part in the flow of current so their mutual collision becomes significant which causes the increase in resistivity.

References

1. J. Santamaria, I. Martil, E. Iborra, G. G. Diaz, F. S. Queada, Solar Energy Matter **28** (1990) 31.
2. S. N. Sahu, S. Chandra, Solar Cells, **22** (1987) 163.
3. J. W. Orton, B. J. Goldsmith, J. A. Chapman, M. A. Powell, Appl. Phys., **53** (1982) 1602.
4. N. A. Shah, A. K. S. Aqili, A. Maqsood, Journal of Crystal Growth **290** (2006) 452.
5. E. D. Palik, Handbook of Optical Constants of Solids II, Academic Press, San Diego, USA, (1991).
6. J. M. Magn, Mater. **152** (1996) 159.
7. V. Kapaklis, P. Poulopoulos, V. Karoutsos, T. Manouras, C. Politis, Thin Solid Films **510** (2006) 138.
8. K. L. Chopra, Thin Film Phenomena, McGraw-Hill, New York (1969).
9. Z. Leipzig, Phys. Chem. **31** (1935) 157.
10. J. P. Enrquez, X. Mathew, Solar Energy Materials & Solar Cells **76** (2003) 313.
11. K. Ravichandran, P. Philominathan, Applied Surface Science **255** (2009) 5736.
12. S. K. Ghandghi. VLSI Fabrication Principles, Wiley New York, (1994).
13. M. Ristova, M. Ristov, Applied Surface Science **181** (2001) 68.
14. H. You, R. P. Chiarello, H. K. Kim, K. G. Vandervoort, Phys. Rev. Lett. **70** (1993) 2900.
15. A. Iwamoto, T. Yoshinobu, H. Iwasaki, Phys. Rev. Lett. **72**. (1994) 4025.
16. G. W. Mbise, G. A. Niklasson, C. G. Granqvist, Solid State Commun. **97** (1996) 965.
17. V. Popescu, E. M. Pica, I. Pop, R. Grecu, Thin Solid Films, **349** (1999) 67.
18. R. Swanepoel, J. Phys. E:Sci.Instrum. **6** (1983) 1214.
19. A. U.Ubale, et al. Turk J. Phys **31** (2007) 279.
20. M. Ristova, M. Ristov, Applied Surface Science **181** (2001) 68.
21. S. J. Ikhmayies, R. N. Ahmad-Bitar, American Journal of Applied Sciences **5** (2008) 1141.
22. E. Bertmana, J. L. Morenzaa and J. Estevea, Thin Solid Films **123** (1985) 297.

CONCLUSION

The present work demonstrates the preparation of cadmium sulfide (CdS) thin films, Ag-doped CdS thin films and study of their physical properties with the help of different characterization tools. The equipment (CSS) for the fabrication of thin films was assembled and installed at *Thermal Transport Laboratory, SCME, NUST*. The experimental results showed that for as deposited CdS films prepared by CSS technique have high electrical resistivity ~ 2.67×10^{8} Ω-cm. The experimental results also showed that the resistivities of the films decreased with the increase of film thickness and Ag-concentration. The electrical resistivity of CdS thin films with doping of Ag atoms, dropped up to several orders of magnitude i.e. 2.180×10^{3} Ω-cm. The value of resistivity could be decreased with increase in more silver ratio in CdS thin films. Thin films of CdS prepared by CSS technique showed polycrystalline structure with preferred growth in <111> direction. Structural investigation showed that average grain size increased from *195.7* nm to *409.5* nm with increase in film thickness from *248* nm to *860* nm, respectively. Optical study showed that optical transmission decreased with increase in silver mass % because silver is a good reflector. Transmission decreased from *50-80%* to *40-70%* as samples were doped with silver. The important factor is to decrease resistivity of films but not at the cost of transmission loss so that it can be used efficiently in opto-electronic devices i.e. solar cells.

Regarding future work, CSS apparatus will be modified for fabrication of thin films of controlled thickness. Electrical properties will be measured for range of temperature (77K to 300K) at Ecopia HMS-5000 Hall effect measurement system, which is installed recently at *Thermal Transport Laboratory, SCME, NUST*. Thin films of other materials (II-VI) like CdTe, ZnS, ZnTe will be studied for similar physical properties in comparison with CdS thin films. Fabrication of thin film solar cell (CdS/CdTe) and study of its opto-electic properties are included in future goals.